Joint Optimization of Multi-Vehicles and Traffic Signal: A Parallel Approach in Spatial Domain

Jichen Zhu, Haoran Wang, *Member, IEEE*, Heye Huang, Xiaoguang Yang, Chaopeng Tan, Jia Hu, *Senior Member, IEEE*

***Abstract*—With the emerging Internet of Things (IoT) and Vehicle-Road-Cloud Integration System (VRCIS) technologies, coordinating Connected and Automated Vehicles (CAVs) and traffic signal is becoming a practical solution to further enhance traffic efficiency. However, current studies still have limitations. Firstly, there is a domain mismatch between CAV trajectory planning (temporal domain) and signal optimization (spatial domain). This mismatch requires separate modeling of trajectory planning and signal optimization, which greatly reduces global optimality. Secondly, previous studies are not applicable to actual mixed traffic environment, since they mostly simplify Human-driven Vehicle's (HV) behavior without considering queuing and stop-and-go maneuvers. Therefore, we propose a novel Multi-Vehicles and Signal Cooperation (MVSC) planner to solve the limitations via following designs. (i) Joint optimization is achieved via formulating in the spatial domain, unifying CAV's planning domain with traffic signal optimizing domain. (ii) A parallel algorithm is designed for the adaptation to numbers of CAVs. This algorithm is based on Alternating Direction Method of Multipliers (ADMM), making full use of IoT and VRCIS. (iii) HV queuing and stop-and-go behaviors are considered in our modeling. Simulation results show that the proposed MVSC planner can enhance efficiency and ecology by 23.60% and 15.63%. At CAV's penetration rate of 40% and V/C ratio of 0.75, the proposed planner shows its full potential in performance enhancement. The average computation time of parallel computing approach is only within 10 milliseconds, which confirms the real-time implementation capability.**

***Index Terms*—Vehicle-signal cooperative optimization, Spatial domain vehicle dynamics, Parallel distributed computation, Mixed traffic environment.**

I. Introduction

THE signalized intersection represents a key bottleneck of urban transportation, leading to a 5% to 10% more time delay [1] and a 14% increase in fuel consumption [2]. In recent years, the emerging Internet of Things (IoT) and Vehicle-Road-Cloud Integration System (VRCIS) technologies enable the cooperation in vehicle-to-vehicle and vehicle-to-signal [3], [4]. With the increasing penetration of Connected and Automated Vehicles (CAVs), the IoT environment has great potential to alleviate urban congestion, enhance traffic safety, and reduce emissions through the cooperative decision-making of multi-vehicles trajectory planning and traffic signal plan optimization [5], [6]. It coordinates CAV trajectory and signal timing plan to generate smooth vehicle progression and enhance signal control efficiency. However, the cooperative decision-making problem of vehicles and the traffic signal still faces three challenges.

Firstly, conventional cooperative decision-making methods are difficult to simultaneously optimize vehicle trajectory and traffic signal timing, which greatly reduce global optimality. The rationale is that there is a modeling mismatch between vehicle trajectory planning and signal timing. In the traffic signal optimization, the time of phase switching is the decision variable [7]. In contrast, in vehicle trajectory planning problems, decision variables typically are the acceleration, speed or spatial position respect to the time [8], [9]. Therefore, the time is an independent variable and cannot be optimized in conventional trajectory model based on the temporal domain [10]. It means signal timing variables cannot be optimized in the vehicle trajectory planning problem directly. Therefore, conventional studies always separate trajectory planning and signal optimization. They mostly formulate the problem into a bi-level optimization (or two-stage) problem [11]. Signal optimization is the upper-level (or first stage) problem, where time is a decision variable. The objective is to optimize the signal plan to maximize overall intersection efficiency based on estimated vehicle trajectory [12], [13]. Vehicle trajectory planning is the lower-level (or second stage) problem, which is formulated in the temporal domain. It aims to adjust CAV trajectory to realize cooperative driving under the optimized signal plan. This bi-level scheme cannot handle the limitation that vehicles' trajectory planning would in return make the input signal timing not optimal and even infeasible [14]. To address this modeling mismatch, recent studies adopted the spatial domain-based trajectory planning method, where vehicle arrival time at each position is an optimization variable [15], [16]. In the spatial domain vehicle model, time is treated as a decision variable rather than an independent domain, allowing it to be jointly optimized with traffic signal control. For example, Tian et al. [17] formulated the vehicle arrival time at each spatial position as a decision variable, providing an effective tool to handle spatially dependent constraints in

This paper is partially supported by National Key R&D Program of China (No. 2022YFF0604905), National Natural Science Foundation of China (Grant No. 52472350 and 52302412), the State Key Lab of Intelligent Transportation System under Project (2025-A002), Yangtze River Delta Science and Technology Innovation Joint Force (2023CSJGG0800), and Shanghai Sailing Program (No. 23YF1449600). *(Corresponding author: Haoran Wang)*

Jichen Zhu, Haoran Wang, Xiaoguang Yang, and Jia Hu are with Key Laboratory of Road and Traffic Engineering of the Ministry of Education, Tongji University, No.4800 Cao'an Road, Shanghai, 201804, China. (e-mail: jichen_zhu@tongji.edu.cn, wang_haoran@tongji.edu.cn, yangxg@tongji.edu.cn, hujia@tongji.edu.cn)

Heye Huang is with the Connected and Autonomous Transportation Systems Laboratory, University of Wisconsin–Madison, Madison, WI 53715 USA. (email: hhuang468@wisc.edu)

Chaopeng Tan is with the Department of Transport and Planning, Delft University of Technology, Gebouw 23, Stevinweg 1, 2628 CN, Delft, Netherlands. (email: c.tan-2@tudelft.nl)

vehicle trajectory planning. Li et al. [18] developed a trajectory model to generate the passing time window at each spatial position for CAVs, enabling ecological driving at the actuated signalized intersection. The spatial domain vehicle trajectory model provides a promising method for the joint optimization of vehicle trajectories and traffic signal timing.

Secondly, conventional studies' computing efficiency is concerned when there is a growing number of CAVs. Due to the interaction between vehicles, previous cooperative decision-making algorithms follow a centralized scheme to generate all vehicles' trajectories at the same time [19], [20], [21]. When the number of CAVs increases, interactions between multiple CAVs are significantly amplified. The optimization complexity exponentially increases [22]. Hence, the centralized planning scheme may not be applicable anymore for multi-CAVs' cooperation with the traffic signal. Some state-of-the-art studies inspire us to develop a distributed method for the cooperation of large-scale CAVs. The first approach is multi-agent learning, which does not rely on control models and instead extracts insights from accumulated experiences [23], [24]. However, this method relies heavily on training data and may perform unreliably in highly dynamic traffic environments. Another practice is using parallel optimization algorithms. For instance, operator splitting methods [25], Alternating Direction Method of Multipliers (ADMM) [26], parallel particle swarm [27] have been proposed. Most existing studies on parallel algorithms focus on the trajectory planning problem. This paper investigates the application of parallel algorithms to enable efficient cooperative decision-making between large-scale CAVs and the traffic signal.

Thirdly, existing studies tend to simplify HV behavior, making them unable to effectively adapt to the mixed traffic environment. Past studies mostly focus on a 100%-CAV traffic environment [28], [29]. However, Human-driven Vehicle (HV) would still exist and last for a long time [30]. In the CAV and HV mixed traffic environment, the behavior of HV is a critical factor that shall be considered. Some studies assume that CAV can arrive at the stop line exactly at the beginning of the green time and lead the HV to pass the intersection [31]. However, such assumptions may not hold in practice, as CAVs can be intermittently obstructed by HVs and cannot arrive at the stop line exactly at the expected time. To address this challenge, a few studies incorporate the behavior of the preceding HV ahead of the CAV, and try to avoid CAV collisions with preceding HV by ensuring a safe following distance [32]. However, the planned trajectories of CAVs and signal plan may in turn affect the behavior of HVs, making it difficult to accurately predict their trajectories. In particular, existing studies often overlook the impact of vehicle queuing and stop-and-go dynamics at intersections, assuming all HVs can pass through the intersection within a single green phase [33]. Such assumptions may result in infeasible CAV trajectories when unexpected HV stops or queue spillbacks occur, and can also lead to suboptimal signal plans that increase HV delay.

To address these limitations, we propose a Multi-Vehicles and Signal Cooperation (MVSC) planner in this study. It is highlighted by proposing a vehicle dynamic model based on the spatial domain to enable integrated optimization of trajectory planning and signal optimization. We also propose a parallel distributed computing approach based on Alternating Direction Method of Multipliers (ADMM) method to accelerate model computation. The main contributions of this study are as follows:

- **Ensuring global optimality by jointly optimizing all CAVs' trajectories and signal timing**: This is achieved by our proposed model formulation in the spatial domain, where the CAV's arrival time at each position is now an optimization variable. Unlike conventional vehicle dynamic models in the temporal domain, the time is no longer an independent variable and can be optimized within the signal control problem. We formulate vehicle dynamics in the spatial domain and develop the joint optimization problem. It is capable of finding global optimal solutions that give consideration to both CAV individual's mobility and global traffic efficiency.
- **Effectively solving the problem using a parallel algorithm within the context of IoT**: We propose a parallel distributed computing approach based on the ADMM method. This approach transforms a centralized optimization problem into multi-subproblems. It combines the interaction between vehicles and road infrastructures in the IoT environment. All subproblems could be solved via a distributed approach on each computing module. Moreover, a concomitant iteration scheme is proposed to solve the problem along with the rolling horizon execution. These designs would accelerate the computation time and enable real-world implementation, making full use of IoT and VRCIS.
- **Adaptive to CAV and HV mixed traffic:** Our proposed MVSC planner explicitly considers HV behavior to avoid potential conflicts between CAVs and HVs. To better capture HV dynamics, we incorporate vehicle queuing and stop-and-go behavior into the HV modeling process. It is beneficial to generate feasible CAV trajectories and efficient signal plan.

The remainder of this paper is organized as follows. Section II describes the system structure of the proposed planner. Section III introduces the problem formulation of cooperative decision-making. To efficiently solve the problem, we propose a parallel distributed computing approach with the concomitant iteration scheme in Section IV. Section V evaluates the proposed planner by simulation experiments. Section VI concludes this research and proposes future research directions.

II. System Structure

The proposed MVSC planner is highlighted for cooperative decision-making of multi-CAVs and the traffic signal. It jointly optimizes multi-CAVs' trajectories and the traffic signal timing by formulating the cooperative decision-making problem in the spatial domain. Real-time computational efficiency is ensured by a parallel distributed computing approach. We use $V, V_{\mathrm{A}}, V_{\mathrm{H}}$ to denote the set of all vehicles, set of CAVs, and set of HVs. In the mixed traffic environment,

we have $V = V_{\mathrm{A}} \cup V_{\mathrm{H}}$. We use $\mathcal{E}$ to denote all pairwise adjacent vehicles, and each vehicle needs to ensure a safe headway with its preceding vehicle.

The proposed MVSC planner is adopted for the scenario as illustrated in Fig. 1. (a). In this scenario, CAVs and HVs are mixed and aim at efficiently passing through the intersection. It is assumed that all vehicles are already in their desired lanes and do not need lane changing, which is a common practice in many existing studies [9], [27]. The intersection is regulated by a Traffic Signal Controller (TSC). Real-time traffic data could be collected by Roadside Traffic Detector (RTD) and will be sent to Road Computing Unit (RCU). CAV's trajectory is planned by Onboard Unit (OBU). Communication is enabled among CAVs, RCUs, and TSC. It combines the interaction between vehicles and road infrastructures in the IoT environment [34], [35]. In this study, we assume an ideal communication environment where the information exchange among CAVs, RCUs, and TSC is timely and accurate.

Fig. 1. (b) shows the computation network of the MVSC planner. It consists of four types of computing modules: CAV planner, signal controller, roadside adapter, and coordinator. CAV planner, signal controller, and roadside adapter are responsible for parallelly optimizing subproblems. Coordinator is designed to realize the consensus among different computing modules. Details of the four modules are presented as follows.

- **CAV planner ($\mathbb{V}_i$)**: CAV planner is equipped on the OBU. It is used for optimizing trajectory of individual CAV $i \in V_{\mathrm{A}}$. The planning objective is to enhance driving mobility and passing through the intersection without stopping.
- **Signal controller ($\mathbb{S}$)**: Signal controller is equipped on the TSC. It aims at optimizing signal plan to minimize global traffic delay. The optimized signal timing plan also serves as a constraint for CAV's trajectory planning.
- **Roadside adapter ($\mathbb{R}_e$)**: Roadside adapter is equipped on the RCU. It adjusts CAV's trajectory to avoid collisions with surrounding vehicles. Each adjacent vehicle pair is denoted by $e \in \mathcal{E}$ and will be allocated to a computing recourse in RCU.
- **Coordinator ($\mathbb{G}_i$ and $\mathbb{G}_s$)**: The coordinator is equipped on the RCU. It aims at reaching the consensus among all the aforementioned three modules. The signal coordinator $\mathbb{G}_s$ is responsible for updating and broadcasting consensus variables of the signal timing among $\mathbb{V}_i$ and $\mathbb{S}$. The vehicle coordinator $\mathbb{G}_i$ is responsible for updating and broadcasting consensus variables of CAVs' control inputs among $\mathbb{V}_i$, $\mathbb{S}$, and $\mathbb{R}_e$.

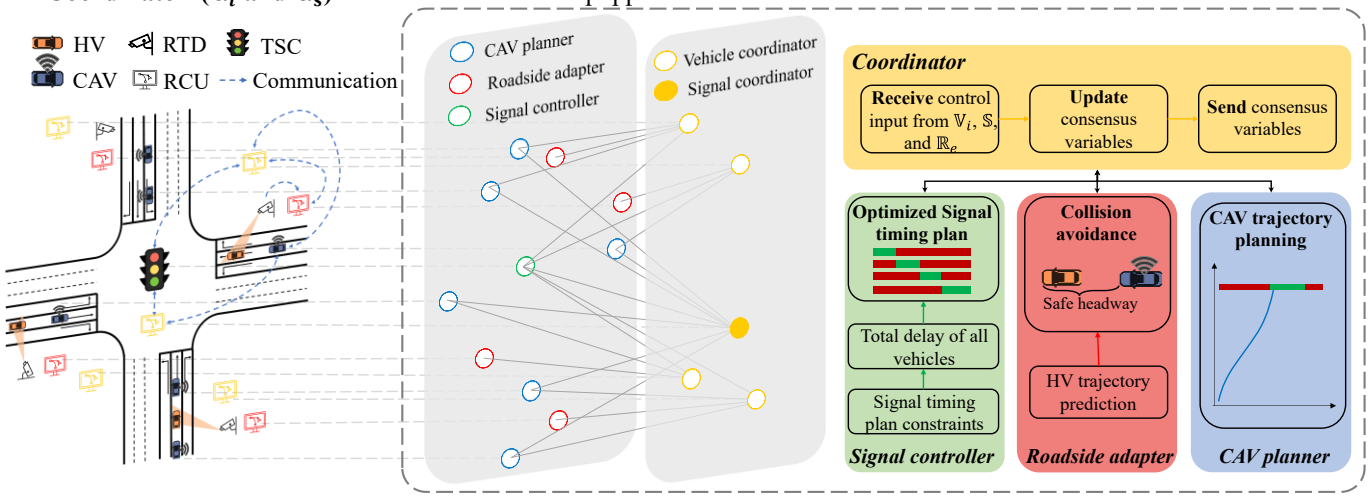

(a) The traffic scenario (b) MVSC computation network

Fig. 1. System structure of the proposed MVSC controller within the context of IoT.

III. Problem Formulation

The cooperative decision-making problem is formulated into a joint optimization of both CAV trajectory planning and traffic signal control in the MVSC planner. The joint optimization is achieved by novelly formulating in the spatial domain. The main variables are listed in Section Appendix.

A. Definition of the Spatial Domain

Spatial domain is defined as shown in Fig. 2. (a). The spatial domain utilizes longitudinal distance as the independent domain. In the spatial domain, the road link is divided into several segments of length Δx, with each segment k representing a discrete cross-section. We use the K to denote the position index of the stop line. The trajectory of vehicle i is a function of space step (i.e., discrete cross-section) k. Vehicle i's arriving time $t_{i,k}$ at space step k could be optimized. Hence, a CAV i's arrival time at the stop line $t_{i,K}$ could be optimized in trajectory planning. For example, $t_{i,K}$ should be constrained by signal timing, such as passing the intersection after the beginning of green duration t_p^{b} and before the ending of green duration t_p^{e} (i.e., $t_p^{\mathrm{b}} \le t_{i,K} \le t_p^{\mathrm{e}}$). Therefore, the vehicle trajectory planning can be integrated into the signal optimization problem.

However, in the conventional temporal domain as shown in Fig. 2. (b), time t is the independent variable. In the temporal domain-based trajectory planning, time cannot be optimized. Hence, the start of green light cannot be introduced into the trajectory planning directly. Joint optimization of CAV trajectory planning and signal timing cannot be directly achieved.

Compared with the temporal domain vehicle dynamic formulation, the spatial domain-based model uses longitudinal distance as the independent variable, making the arrival time at each position a decision variable that can be jointly optimized with signal timing. This allows signal constraints to be directly incorporated into trajectory planning, whereas temporal domain-based models treat time as fixed and require constraint approximation or bi-level structures [14].

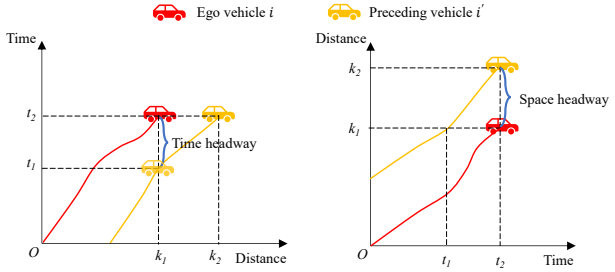

(a) Spatial domain (b) Temporal domain

Fig. 2. A comparison between spatial and temporal domain.

Furthermore, the spatial domain is good at enhancing traffic stability. As shown in Fig. 2. (a), ego-vehicle i is following its preceding vehicle i'. In the spatial domain, the future trajectory of the preceding vehicle i' could be utilized as a path-preview. The ego-vehicle i could react to the preceding vehicle i' in advance. However, as shown in Fig. 2. (b), the ego-vehicle i has to react to the preceding vehicle i' hysteretically. This strength of spatial domain could be justified in recent studies on vehicle platooning [36].

B. State and Control Definition

Definition 1 (Vehicle state vector $\boldsymbol{\xi}_i$): The state of vehicle i includes the vehicle arrival time and speed in the spatial domain:

$$\boldsymbol{\xi}_i = \begin{bmatrix} \boldsymbol{t}_i \\ \boldsymbol{\pi}_i \end{bmatrix} \tag{1}$$

where $\boldsymbol{t}_i = [t_{i,1}, \dots, t_{i,k}, \dots]$ is the arrival time vector of vehicle i at each space step k; $\boldsymbol{\pi}_i = [\pi_{i,1}, \dots, \pi_{i,k}, \dots]$ is the vector of the reciprocal of speed of vehicle i at each space step k, defined in Equation (2). k is the index of space step, representing the index of discrete cross-section.

$$\pi_{i,k} = \frac{1}{v_{i,k} + \sigma} \tag{2}$$

where $v_{i.k}$ is the speed of vehicle i at the space step k; σ is an extremely small positive value. In the scenario of interest, we have $v_i \geq 0$.

Definition 2 (Vehicle control vector $\boldsymbol{u}_i$): The control variable of vehicle i is defined as follows:

$$\boldsymbol{u}_i = [\boldsymbol{a}_i] \tag{3}$$

where $\boldsymbol{a}_i = [a_{i,1}, \dots, a_{i,k}, \dots]$ is the acceleration vector of vehicle i at each space step k.

Definition 3 (Signal state vector $\boldsymbol{\xi}_s$): For the signal controller, the state is defined as the total delay of vehicles (including both CAVs and HVs). The delay of vehicle i is calculated as the extra time needed compared with the expected travel time at free flow speed without stops.

$$\boldsymbol{\xi}_s = \left[\left\{t_{i,K} - t_{i,K}^{\exp}\right\}_{\forall i \in V}\right]^T \tag{4}$$

where $t_{i,K}^{\exp}$ is the expected arrival time at free flow speed of vehicle i at the stop line position K. The $t_{i,K}$ is the actual arrival time of vehicle i at the stop line position K. V represents the set of all vehicles.

Definition 4 (Signal control vector $\boldsymbol{u}_s$): The signal control vector consists of the green duration beginning time of each phase p (t_p^{b}), the green duration ending time of each phase p (t_p^{e}), and the cycle length (C).

$$\boldsymbol{u}_s = \left[\left\{t_p^b, t_p^e\right\}_{\forall p \in P}, C\right]^T \tag{5}$$

where t_p^{b} and t_p^{e} are the beginning and ending time of green duration of phase p, respectively; and P is the set of all phases of the signal plan.

C. Vehicle Dynamics Modeling in the Spatial Domain: $\mathbb{D}_A$

In the conventional temporal domain, the longitudinal vehicle kinematics model is generally formulated as follows:

$$\frac{dx}{dt} = v \tag{6}$$

$$\frac{dv}{dt} = a \tag{7}$$

Since $v \geq 0$ in the scenario of interest, Equation (6) could be transformed into Equation (8).

$$\frac{dt}{dx} = \frac{1}{v + \sigma} \tag{8}$$

Introducing equation (8) into Equation (7), we have:

$$\frac{d\frac{1}{v+\sigma}}{dx} = -\frac{1}{(v+\sigma)^2}\frac{dv}{dx} = -\frac{1}{(v+\sigma)^2}\frac{dv}{dt}\frac{dt}{dx} = -\frac{1}{(v+\sigma)^3}a \tag{9}$$

We define the slowness as $\pi = \frac{1}{v+\sigma}$. Then Equations (8) and (9) can be reformulated as:

$$\frac{dt}{dx} = \pi \tag{10}$$

$$\frac{d\pi}{dx} = -\pi^3 a \tag{11}$$

Equations (10) and (11) are discretized based on Euler method. Equations (12) and (13) are the final form of the vehicle dynamics model in the spatial domain [15], [18]

$$t_{i,k+1} = t_{i,k} + \pi_{i,k}\Delta x, k = k_i, k_i + 1, \dots, K - 1 \tag{12}$$

$$\pi_{i,k+1} = \pi_{i,k} - \pi_{i,k}^3 a_{i,k}\Delta x, k = k_i, k_i + 1, \dots, K - 1 \tag{13}$$

where Δx is the length of a space step; k_i is the initial space step of vehicle i; and K is the position index of the stop line.

The non-linear vehicle dynamic Equation (13) will make the problem non-convex and hard to solve. To ensure the model is convex, we linearized Equation (13). The basic idea of the linearization is using first-order Taylor approximation. In the rolling horizon control framework, we can move one space step forward of the previous optimized control input to generate a seed trajectory $(\pi_{i,k}^0, a_{i,k}^0)$ [37]. The seed trajectory from the last step can be considered as the initial solution to the current problem. The first order Taylor approximation of Equation (13) at $(\pi_{i,k}^0, a_{i,k}^0)$ is:

$$\begin{aligned} \pi_{i,k+1} = \pi_{i,k} - \left(\pi_{i,k}^0\right)^3 a_{i,k}^0 \Delta x - 3\left(\pi_{i,k}^0\right)^2 a_{i,k}^0 \Delta x \cdot \left(\pi_{i,k} - \pi_{i,k}^0\right) \\ - \left(\pi_{i,k}^0\right)^3 \Delta x \cdot \left(a_{i,k} - a_{i,k}^0\right), \\ k = k_i, k_i + 1, \dots, K - 1 \end{aligned} \tag{14}$$

D. Objective Function

The objective of the proposed MVSC controller is to enhance global traffic efficiency and individual CAVs' mobility. Hence, the objective function is formulated as Equation (15). It includes two parts, the cost of CAVs' mobility J_i (Equation (16)) and the cost on global traffic efficiency J_s (Equation (17)).

$$\min J = \alpha_1 \sum_{i \in V_A} J_i + \alpha_2 J_s \tag{15}$$

$$J_i = \sum_{k=k_i}^{K} \underbrace{\left(\beta_1 \left\| v_{i,k} - v_{i,k}^{\exp} \right\|^2 + \beta_2 \left\| a_{i,k} \right\|^2\right)}_{\text{running cost}} + \underbrace{\beta_3 \left(t_{i,K} - t_{i,K}^{\exp}\right)}_{\text{terminal cost}}, \forall i \in V_A \tag{16}$$

$$J_s = \sum_{i \in V} \left(t_{i,K} - t_{i,K}^{\exp}\right) \tag{17}$$

where α_1 and α_2 are cost weighting factors of the main objective J; β_1, β_2, and β_3 are cost weighting factors of CAVs' mobility objective J_i; $v_{i,k}^{\exp}$ is the expected speed of CAV i at space step k with free flow speed; $t_{i,K}^{\exp}$ is the expected arrival time of CAV i at stop line K.

CAV's trajectory planning objective J_i is to minimize running cost and terminal cost. The running cost includes state error cost and control effort cost. Terminal cost is designed to reduce CAV's delay to ensure driving mobility. Signal controller's objective is to minimize all vehicles' total delay to enhance overall traffic efficiency.

E. Constraints

Constraints of the MVSC controller consist of signal timing constraint ($\mathbb{C}_S$), collision avoidance constraint with preceding CAV ($\mathbb{C}_{C,CAV}$) and HV ($\mathbb{C}_{C,HV}$), CAV's execution capability constraint ($\mathbb{C}_E$), and CAV's non-stop driving constraint ($\mathbb{C}_N$). The formulation of these constraints is presented in the following.

1) Signal timing constraint $\mathbb{C}_S$: In this study, the signal phase sequence is fixed and shown in Fig. 3. The beginning and ending time of each phase and cycle length could be optimized for enhancing traffic efficiency. The signal timing plan can be easily extended to accommodate flexible phase sequence and combination.

$$g_{\min} \le t_p^{e} - t_p^{b} \le g_{\max}, \forall p \in P \tag{18}$$

$$t_{p+1}^{b} = t_p^{e} + l, \forall p \in P \tag{19}$$

$$\sum_{p \in P} \left(t_p^{e} - t_p^{b}\right) + L = C \tag{20}$$

$$C_{\min} \le C \le C_{\max} \tag{21}$$

where $g_{\min}$ and $g_{\max}$ denote the minimum and maximum green duration; l is the loss time and inter-green time between phase switch process; L is the total loss time and inter-green time in a cycle; $C_{\min}$ and $C_{\max}$ denote the minimum and maximum cycle length.

In this study, the signal plan follows a conventional cycle structure. This choice aligns with the operational rules of most existing signal control systems, facilitating direct comparison with conventional control methods. In addition, the signal optimization can be easily extended to the flexible signal scheme without a fixed phase structure and sequence [7].

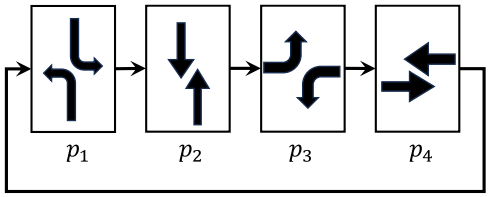

Fig. 3. Illustration of the signal timing strategy.

2) Collision avoidance constraint with preceding CAV $\mathbb{C}_{C,CAV}$: The trajectory planning of CAV i should avoid collisions with its preceding vehicle i'. The preceding vehicle i' could be either a CAV or HV. When it is a CAV, $t_{i',k}$ is a state variable of the system. Both the two CAVs' trajectories should be constrained by the safe following time headway:

$$t_{i,k} - t_{i',k} \ge t_{\text{safe}}, \forall (i,i') \in \mathcal{E}, i \in V_A, i' \in V_A, k = k_i, k_i + 1, \dots, K \tag{22}$$

where $\mathcal{E}$ is the set of all pairwise adjacent vehicles in the intersection. The adjacent pairwise vehicles are denoted as (i, i'), where i is the following vehicle and i' is the preceding vehicle. t_{safe} is the safe time headway threshold.

3) Collision avoidance constraint with preceding HV: $\mathbb{C}_{C,HV}$: If the preceding vehicle of CAV i is an HV i', the roadside adapter first predicts the HV's trajectory using the Intelligent Driver Model (IDM) in the conventional temporal domain [38]. This predicted trajectory is then transformed into the spatial domain and used for collision avoidance constraints.

The future trajectories of HVs are predicted based on the IDM as follows:

$$a_{i'}(t) = a_{\max}\left[1 - \left(\frac{v_{i'}(t)}{v_0}\right)^{\delta} - \left(\frac{s^*\left(v_{i'}(t), \Delta v_{i'}(t)\right)}{s_i}\right)^2\right], \quad \forall i' \in V_H \tag{23}$$

where $a_{i'}(t)$ is the acceleration of HV i' at time step t; $a_{\max}$ is the maximum acceleration/deceleration; $v_{i'}(t)$ is the speed of HV i' at time step t; v_0 is the desired speed; δ is the parameter of acceleration exponent; $s_{i'}$ is the spacing between the HV i' and its preceding vehicle; $s^*(v_{i'}(t), \Delta v_{i'}(t))$ is the desired minimum gap as follows:

$$s^*\left(v_{i'}(t), \Delta v_{i'}(t)\right) = s_0 + \max\left(0, v_{i'}(t)T + \frac{v_{i'}(t)\Delta v_{i'}(t)}{2\sqrt{a_{\max} a_{\text{comf}}}}\right), \quad \forall i \in V_H \tag{24}$$

where s_0 is the minimum gap of two adjacent vehicles; T is the time desired time headway; $\Delta v_{i'}(t)$ is the speed difference between the HV i' and its preceding vehicle; a_{comf} is the comfortable deceleration.

Although the IDM is defined in the temporal domain, the predicted HV trajectories (i.e., speed and acceleration over time) are subsequently converted into the spatial domain using vehicle kinematic relationships. Specifically, we apply Equations (10) and (11) to derive the $t_{i'}(x)$ and $\pi_{i'}(x)$ at each spatial step k. This transformation allows the predicted HV

trajectory to be fully compatible with our spatial-domain formulation, enabling consistent modeling of CAV-HV interactions in the same domain. It is also important to note that the predicted trajectories of HVs are treated as fixed parameters rather than decision variables in the optimization problem. This ensures that the spatial-domain controller maintains modeling consistency without modeling mismatch.

Traditional IDM cannot describe the vehicle queuing during the red light. We adopt the formulation proposed by [9], which treats the red signal as a phantom vehicle located at the stop line, allowing the IDM to capture queuing dynamics during red phases. HVs decelerate as they approach the red light, similar to following a stopped vehicle. This extension enables a more realistic representation of queuing behavior at signalized intersections, improving the accuracy of HV trajectory prediction and enhancing the applicability of the model in mixed traffic environments.

When the trajectory of preceding HV $i' \in V_{\mathrm{H}}$ is predicted, we can constrain the CAV i's trajectory to ensure the safe time headway as follows:

$$t_{i,k} - t_{i',k} \geq t_{\mathrm{safe}}, \forall (i,i') \in \mathcal{E}, i \in V_{\mathrm{A}}, i' \in V_{\mathrm{H}}, \quad k = k_i, k_i+1, \dots, K \tag{25}$$

where $t_{i',k}$ $(i' \in V_{\mathrm{H}})$ is a predicted parameter by the extended IDM.

This study uses a deterministic car-following model (i.e., IDM) for predicting HV trajectories. Stochastic car-following models that quantify the uncertainty in HV behaviors can be easily incorporated into the proposed planner.

4) CAV's execution capability constraint $\mathbb{C}_{\mathrm{E}}$: The CAV's speed and acceleration should be constrained in a rational range:

$$\pi_{i,k} \geq \frac{1}{v_{\max}}, k = k_i, k_i+1, \dots, K, \forall i \in V_{\mathrm{A}} \tag{26}$$

$$a_{\min} \leq a_{i,k} \leq a_{\max}, k = k_i, k_i+1, \dots, K, \forall i \in V_{\mathrm{A}} \tag{27}$$

where $v_{\max}$ is the maximum speed of vehicle; $a_{\min}$ and $a_{\max}$ are the minimum deceleration and maximum acceleration, respectively.

5) CAV's non-stop driving constraint $\mathbb{C}_{\mathrm{N}}$: To enhance the driving mobility of CAV, CAV's trajectory planning should be constrained to pass through without stops at the stop line.

$$t_{p_i}^{\mathrm{b}} \leq t_{i,K} \leq t_{p_i}^{\mathrm{e}}, \forall i \in V_{\mathrm{A}} \tag{28}$$

where p_i is the corresponding signal phase of CAV i. If the CAV i cannot pass the intersection at the current cycle, $t_{p_i}^{\mathrm{b}}$ and $t_{p_i}^{\mathrm{e}}$ in Equation (27) will be replaced by the beginning and ending time of phase p_i in the next cycle.

F. Overall Formulation

The overall formulation of jointly planning CAVs' trajectory and signal timing is integrated into (29).

$$\min J = \alpha_1 \sum_{i \in V_{\mathrm{A}}} J_i + \alpha_2 J_{\mathrm{s}}$$

subject to:

$$\begin{gathered} \mathbb{D}_{\mathrm{A}}(\boldsymbol{u}_i, \boldsymbol{u}_{\mathrm{s}}) \text{: Equations (12) and (14)} \\ \mathbb{C}_{\mathrm{S}}(\boldsymbol{u}_{\mathrm{s}}) \text{: Equations (18)–(21)} \\ \mathbb{C}_{\mathrm{C,CAV}}(\boldsymbol{u}_i) \text{: Equation (22)} \\ \mathbb{C}_{\mathrm{C,HV}}(\boldsymbol{u}_i) \text{: Equation (25)} \\ \mathbb{C}_{\mathrm{E}}(\boldsymbol{u}_i) \text{: Equations (26) and (27)} \\ \mathbb{C}_{\mathrm{N}}(\boldsymbol{u}_i) \text{: Equation (28)} \end{gathered} \tag{29}$$

IV. Problem Solving

The time complexity of the centralized problem (29) is $\mathcal{O}((n \times n_s)^{\varphi})$, where n is the total number of CAVs, n_s is the length of planning horizon, and φ is the exponent of the solving algorithm [26]. It could be found that with the increase of CAV number n, the time complexity of the centralized problem (29) increases exponentially. Hence, this centralized problem is computationally inefficient for multi-CAVs.

However, CAVs are equipped with onboard computing power, which has been wasted in conventional centralized method. Hence, this paper transforms the conventional centralized problem into multiple parallel distributed decision-making subproblems, to ensure the implementation for large-scale CAVs scenario.

We start this section by introducing the standard Alternating Direction Method of Multipliers (ADMM) algorithm. Then, we will reformulate the centralized problem (29) into the standard form and further propose a novel iteration scheme.

A. The ADMM algorithm for consensus problems

In a distributed system with N controllers, optimization problems are often formulated as a consensus problem:

$$\min \sum_{i=1}^{N} F_i(x_i) \quad \text{subject to:} \quad x_i = z, \forall i = 1, \dots, N \tag{30}$$

where x_i represents the local control variable of controller i, z denotes the global consensus variable.

Its scaled augmented Lagrangian is defined as:

$$L_{\rho}(x,z,y) = \sum_{i=1}^{N} \left(F_i(x_i) + y_i(x_i - z) + \frac{\rho}{2} ||x_i - z||^2 \right) \tag{31}$$

where y_i is the dual variable of controller i.

The ADMM algorithm solves this consensus problem using the following iterations [39]:

$$\begin{gathered} x_i^{m+1} = \operatorname{argmin} L_{\rho}\left(F_i(x_i) + y_i^m(x_i - z^m) + \frac{\rho}{2}||x_i - z^m||^2\right) \\ z^{m+1} = \frac{1}{N}\sum_{i=1}^{N}\left(x_i^{m+1} + \frac{1}{\rho}y_i^m\right) \\ y_i^{m+1} = y_i^m + \rho(x_i^{m+1} - z^{m+1}) \end{gathered} \tag{32}$$

where m is the iteration index.

The consensus form is a standard and well-established way to apply the ADMM algorithm. It allows each subproblem to be solved using specialized solvers or closed-form updates, while the consensus step coordinates the solutions to ensure global feasibility. The ADMM algorithm is not limited to consensus problems; other decomposable formulations could be handled similarly [39].

B. Problem Reformulation into A Consensus Problem

In order to apply the ADMM framework efficiently, problem (29) is reformulated into a consensus form (30) in this section. This transformation introduces local copies of the coupled decision variables, allowing the original problem to

be decomposed into multiple independent subproblems.

The centralized formulation (29) is reformulated through the following steps:

Step 1: Introducing the consensus variable $\boldsymbol{z} = [\boldsymbol{z}_i, \boldsymbol{z}_\mathrm{s}]$ to decompose the centralized formulation (29) into subproblems in terms of each CAV's trajectory planning $J_i^{\mathbb{V}_i}$, signal timing planning $J^{\mathbb{S}}$, and each roadside collision avoiding $J_e^{\mathbb{R}_e}$.

$$\min \hat{J} = \sum_{i\in V_\mathrm{A}} J_i^{\mathbb{V}_i}\left(\boldsymbol{u}_i^{\mathbb{V}_i}, \boldsymbol{u}_\mathrm{s}^{\mathbb{V}_i}\right) + J^{\mathbb{S}}\left(\left\{\boldsymbol{u}_i^{\mathbb{S}}\right\}_{\forall i\in V}, \boldsymbol{u}_\mathrm{s}^{\mathbb{S}}\right) + \sum_{e\in\mathcal{E}}\sum_{i\in V_{\mathrm{A},e}} J_e^{\mathbb{R}_e}\left(\boldsymbol{u}_i^{\mathbb{R}_e}\right) \tag{33}$$

subject to:

$$\boldsymbol{u}_i^{\mathbb{V}_i} = \boldsymbol{z}_i, \boldsymbol{u}_i^{\mathbb{R}_e} = \boldsymbol{z}_i, \boldsymbol{u}_i^{\mathbb{S}} = \boldsymbol{z}_i, \forall e \in \mathcal{E}, \forall i \in V_{\mathrm{A},e}$$
$$\boldsymbol{u}_\mathrm{s}^{\mathbb{V}_i} = \boldsymbol{z}_\mathrm{s}, \boldsymbol{u}_\mathrm{s}^{\mathbb{S}} = \boldsymbol{z}_\mathrm{s}, \forall i \in V_\mathrm{A}$$

where $\boldsymbol{u}_i^{\mathbb{V}_i}$, $\boldsymbol{u}_i^{\mathbb{S}}$ and $\boldsymbol{u}_i^{\mathbb{R}_e}$ are the control vectors of CAV i, in CAV's trajectory planning, signal timing planning, and roadside collision avoiding, respectively. $\boldsymbol{u}_\mathrm{s}^{\mathbb{V}_i}$ and $\boldsymbol{u}_\mathrm{s}^{\mathbb{S}}$ are the signal control vectors in CAV i's trajectory planning and signal timing planning, respectively. $V_{\mathrm{A},e}$ is the set of CAVs corresponding to the adjacent vehicles pair $e \in \mathcal{E}$. In the consensus optimization problem (33), the control variables in different computing modules should be consensus.

Step 2: Transferring the constraints in formulation (29) to indicator functions $\mathbb{I}_\mathrm{A}(\cdot)$, $\mathbb{I}_\mathrm{S}(\cdot)$, $\mathbb{I}_{\mathrm{C,CAV}}(\cdot)$, $\mathbb{I}_{\mathrm{C,HV}}(\cdot)$, $\mathbb{I}_\mathrm{E}(\cdot)$, and $\mathbb{I}_\mathrm{N}(\cdot)$. When the constraint is satisfied, the indicator value is zero, otherwise positive infinity.

$$\mathbb{I}_\mathrm{A}\left(\boldsymbol{u}_i^{\mathbb{V}_i}, \boldsymbol{u}_\mathrm{s}^{\mathbb{V}_i}\right) = \begin{cases} 0, & if\ \left(\boldsymbol{u}_i^{\mathbb{V}_i}, \boldsymbol{u}_\mathrm{s}^{\mathbb{V}_i}\right) \in \mathbb{D}_\mathrm{A} \\ +\infty, & \text{otherwise} \end{cases}, \quad \forall i \in V_\mathrm{A} \tag{34}$$

$$\mathbb{I}_\mathrm{S}\left(\boldsymbol{u}_\mathrm{s}^{\mathbb{S}}\right) = \begin{cases} 0, & if\ \boldsymbol{u}_\mathrm{s}^{\mathbb{S}} \in \mathbb{C}_\mathrm{S} \\ +\infty, & \text{otherwise} \end{cases} \tag{35}$$

$$\mathbb{I}_{\mathrm{C,CAV}}\left(\boldsymbol{u}_i^{\mathbb{R}_e}\right) = \begin{cases} 0, & if\ \boldsymbol{u}_i^{\mathbb{R}_e} \in \mathbb{C}_{\mathrm{C,CAV}} \\ +\infty, & \text{otherwise} \end{cases}, \quad \forall e \in \mathcal{E}, \forall i \in V_{\mathrm{A},e} \tag{36}$$

$$\mathbb{I}_{\mathrm{C,HV}}\left(\boldsymbol{u}_i^{\mathbb{R}_e}\right) = \begin{cases} 0, & if\ \boldsymbol{u}_i^{\mathbb{R}_e} \in \mathbb{C}_{\mathrm{C,HV}} \\ +\infty, & \text{otherwise} \end{cases}, \quad \forall e \in \mathcal{E}, \forall i \in V_{\mathrm{A},e} \tag{37}$$

$$\mathbb{I}_\mathrm{E}\left(\boldsymbol{u}_i^{\mathbb{V}_i}\right) = \begin{cases} 0, & if\ \boldsymbol{u}_i^{\mathbb{V}_i} \in \mathbb{C}_\mathrm{R} \\ +\infty, & \text{otherwise} \end{cases}, \forall i \in V_\mathrm{A} \tag{38}$$

$$\mathbb{I}_\mathrm{N}\left(\boldsymbol{u}_i^{\mathbb{V}_i}\right) = \begin{cases} 0, & if\ \boldsymbol{u}_i^{\mathbb{V}_i} \in \mathbb{C}_\mathrm{N} \\ +\infty, & \text{otherwise} \end{cases}, \forall i \in V_\mathrm{A} \tag{39}$$

Step 3: Introducing indicator functions into objectives.

$$J_i^{\mathbb{V}_i}\left(\boldsymbol{u}_i^{\mathbb{V}_i}, \boldsymbol{u}_\mathrm{s}^{\mathbb{V}_i}\right) = J_i\left(\boldsymbol{u}_i^{\mathbb{V}_i}, \boldsymbol{u}_\mathrm{s}^{\mathbb{V}_i}\right) + \mathbb{I}_\mathrm{A}\left(\boldsymbol{u}_i^{\mathbb{V}_i}, \boldsymbol{u}_\mathrm{s}^{\mathbb{V}_i}\right) + \mathbb{I}_\mathrm{E}\left(\boldsymbol{u}_i^{\mathbb{V}_i}\right) + \mathbb{I}_\mathrm{N}\left(\boldsymbol{u}_i^{\mathbb{V}_i}\right), \forall i \in V_\mathrm{A} \tag{40}$$

$$J^{\mathbb{S}}\left(\left\{\boldsymbol{u}_i^{\mathbb{S}}\right\}_{\forall i\in V}, \boldsymbol{u}_\mathrm{s}^{\mathbb{S}}\right) = J_\mathrm{s}\left(\left\{\boldsymbol{u}_i^{\mathbb{S}}\right\}_{\forall i\in V}, \boldsymbol{u}_\mathrm{s}^{\mathbb{S}}\right) + \mathbb{I}_\mathrm{S}\left(\boldsymbol{u}_\mathrm{s}^{\mathbb{S}}\right) \tag{41}$$

$$J_e^{\mathbb{R}_e}\left(\boldsymbol{u}_i^{\mathbb{R}_e}\right) = \mathbb{I}_{\mathrm{C,CAV}}\left(\boldsymbol{u}_i^{\mathbb{R}_e}\right) + \mathbb{I}_{\mathrm{C,HV}}\left(\boldsymbol{u}_i^{\mathbb{R}_e}\right), \quad \forall e \in \mathcal{E}, \forall i \in V_{\mathrm{A},e} \tag{42}$$

C. Parallel Distributed Computing

The consensus problem (33) is parallelly solved by the ADMM algorithm. Furthermore, we propose a concomitant iteration scheme to accelerate the computation and enhance the adaptation to the dynamic traffic environment.

1) Problem decomposition: To be executed by the computing modules in Fig. 1. within the context of IoT, the consensus problem (33) is decomposed into multi-subproblems, including each CAV's trajectory planning $J_i^{\mathbb{V}_i}$, signal timing planning $J^{\mathbb{S}}$, roadside collision avoiding $J_e^{\mathbb{R}_e}$. The subproblems $J_i^{\mathbb{V}_i}$ are solved by CAV planner $\mathbb{V}_i$. The subproblem $J^{\mathbb{S}}$ is optimized on the signal controller $\mathbb{S}$. The subproblem $J_e^{\mathbb{R}_e}$ is optimized on the roadside adapter $\mathbb{R}_e$.

The scaled augmented Lagrangian function (43) of the consensus problem (33) is:

$$\begin{aligned} L_\rho = & \sum_{i\in V_\mathrm{A}} J_i^{\mathbb{V}_i}\left(\boldsymbol{u}_i^{\mathbb{V}_i}, \boldsymbol{u}_\mathrm{s}^{\mathbb{V}_i}\right) \\ & + \underbrace{\sum_{i\in V_\mathrm{A}} \frac{\rho}{2}\left\|\boldsymbol{u}_i^{\mathbb{V}_i} - \boldsymbol{z}_i + \boldsymbol{\lambda}_i^{\mathbb{V}_i}\right\|^2 + \sum_{i\in V_\mathrm{A}} \frac{\rho}{2}\left\|\boldsymbol{u}_\mathrm{s}^{\mathbb{V}_i} - \boldsymbol{z}_\mathrm{s} + \boldsymbol{\lambda}_\mathrm{s}^{\mathbb{V}_i}\right\|^2}_{\text{Lagrangian function of CAV planner}} \\ & + J^{\mathbb{S}}\left(\left\{\boldsymbol{u}_i^{\mathbb{S}}\right\}_{\forall i\in V}, \boldsymbol{u}_\mathrm{s}^{\mathbb{S}}\right) \\ & + \underbrace{\sum_{i\in V} \frac{\rho}{2}\left\|\boldsymbol{u}_i^{\mathbb{S}} - \boldsymbol{z}_i + \boldsymbol{\lambda}_i^{\mathbb{S}}\right\|^2 + \frac{\rho}{2}\left\|\boldsymbol{u}_\mathrm{s}^{\mathbb{S}} - \boldsymbol{z}_\mathrm{s} + \boldsymbol{\lambda}_\mathrm{s}^{\mathbb{S}}\right\|^2}_{\text{Lagrangian function of signal controller}} \\ & + \sum_{e\in\mathcal{E}}\sum_{i\in V_{\mathrm{A},e}} J_e^{\mathbb{R}_e}\left(\boldsymbol{u}_i^{\mathbb{R}_e}\right) \\ & + \underbrace{\sum_{e\in\mathcal{E}}\sum_{i\in V_{\mathrm{A},e}} \frac{\rho}{2}\left\|\boldsymbol{u}_i^{\mathbb{R}_e} - \boldsymbol{z}_i + \boldsymbol{\lambda}_i^{\mathbb{R}_e}\right\|^2}_{\text{Lagrangian function of roadside adapter}} \end{aligned} \tag{43}$$

where $\boldsymbol{\lambda} = \left[\boldsymbol{\lambda}_i^{\mathbb{V}_i}, \boldsymbol{\lambda}_i^{\mathbb{S}}, \boldsymbol{\lambda}_i^{\mathbb{R}_e}, \boldsymbol{\lambda}_\mathrm{s}^{\mathbb{V}_i}, \boldsymbol{\lambda}_\mathrm{s}^{\mathbb{S}}\right]^\mathrm{T}$ is the scaled dual variable in the augmented Lagrangian function, and ρ is the penalty parameter.

The augmented Lagrangian function (43) is minimized via the following five steps iteratively:

Step 1: At iteration m, computing modules collect the consensus variables $\boldsymbol{z}^{m-1}$ and dual variables $\boldsymbol{\lambda}^{m-1}$ from the last iteration $m-1$.

Step 2: CAV planner $\mathbb{V}_i(\forall i \in V_\mathrm{A})$ solves the following subproblem to update $\boldsymbol{u}_i^{\mathbb{V}_i,m+1}$ and $\boldsymbol{u}_\mathrm{s}^{\mathbb{V}_i,m+1}$:

$$\begin{aligned} \boldsymbol{u}_i^{\mathbb{V}_i,m+1}, \boldsymbol{u}_\mathrm{s}^{\mathbb{V}_i,m+1} = \operatorname{argmin} \Big\{ & J_i^{\mathbb{V}_i}\left(\boldsymbol{u}_i^{\mathbb{V}_i}, \boldsymbol{u}_\mathrm{s}^{\mathbb{V}_i}\right) \\ & + \frac{\rho}{2}\left\|\boldsymbol{u}_i^{\mathbb{V}_i} - \boldsymbol{z}_i^m + \boldsymbol{\lambda}_i^{\mathbb{V}_i,m}\right\|^2 \\ & + \frac{\rho}{2}\left\|\boldsymbol{u}_\mathrm{s}^{\mathbb{V}_i} - \boldsymbol{z}_\mathrm{s}^m + \boldsymbol{\lambda}_\mathrm{s}^{\mathbb{V}_i,m}\right\|^2 \Big\}, \forall i \in V_\mathrm{A} \end{aligned} \tag{44}$$

The signal controller $\mathbb{S}$ solves the following subproblem and update $\boldsymbol{u}_i^{\mathbb{S},m+1}$ and $\boldsymbol{u}_\mathrm{s}^{\mathbb{S},m+1}$:

$$\begin{aligned} \left\{\boldsymbol{u}_i^{\mathbb{S},m+1}\right\}_{\forall i\in V}, \boldsymbol{u}_\mathrm{s}^{\mathbb{S},m+1} = \operatorname{argmin} \Big\{ & J^{\mathbb{S}}\left(\left\{\boldsymbol{u}_i^{\mathbb{S}}\right\}_{\forall i\in V}, \boldsymbol{u}_\mathrm{s}^{\mathbb{S}}\right) \\ & + \sum_{i\in V} \frac{\rho}{2}\left\|\boldsymbol{u}_i^{\mathbb{S}} - \boldsymbol{z}_i^m + \boldsymbol{\lambda}_i^{\mathbb{S},m}\right\|^2 \\ & + \frac{\rho}{2}\left\|\boldsymbol{u}_\mathrm{s}^{\mathbb{S}} - \boldsymbol{z}_\mathrm{s}^m + \boldsymbol{\lambda}_\mathrm{s}^{\mathbb{S},m}\right\|^2 \Big\} \end{aligned} \tag{45}$$

The roadside adapter $\mathbb{R}_e(\forall e \in \mathcal{E})$ solves the following subproblem to update $\boldsymbol{u}_i^{\mathbb{R}_e,m+1}$:

$$\boldsymbol{u}_i^{\mathbb{R}_e,m+1} = \operatorname{argmin}\left\{J_e^{\mathbb{R}_e}\left(\boldsymbol{u}_i^{\mathbb{R}_e}\right) + \frac{\rho}{2}\left\|\boldsymbol{u}_i^{\mathbb{R}_e} - \boldsymbol{z}_i^m + \boldsymbol{\lambda}_i^{\mathbb{R}_e,m}\right\|^2\right\}, \quad \forall e \in \mathcal{E}, \forall i \in V_{\mathrm{A},e} \tag{46}$$

The convex quadratic programming problem in (44)-(46) could be solved with existing optimization algorithms, e.g., interior point method.

Step 3: Update the consensus variable $\boldsymbol{z}$ on the coordinator ($\mathbb{G}_i$ and $\mathbb{G}_\mathrm{S}$):

$$\boldsymbol{z}_i^{m+1} = \frac{\left(\boldsymbol{u}_i^{\mathbb{V}_i,m+1} + \boldsymbol{\lambda}_i^{\mathbb{V}_i,m}\right) + \left(\boldsymbol{u}_i^{\mathbb{S},m+1} + \boldsymbol{\lambda}_i^{\mathbb{S},m}\right) + \sum_{e\in\mathcal{E}_i}\left(\boldsymbol{u}_i^{\mathbb{R}_e,m+1} + \boldsymbol{\lambda}_i^{\mathbb{R}_e,m}\right)}{1 + 1 + \sum_{e\in\mathcal{E}_i} 1}, \quad \forall i \in V_\mathrm{A} \tag{47}$$

$$\boldsymbol{z}_\mathrm{S}^{m+1} = \frac{\sum_{i\in V_\mathrm{A}}\left(\boldsymbol{u}_\mathrm{S}^{\mathbb{V}_i,m+1} + \boldsymbol{\lambda}_\mathrm{S}^{\mathbb{V}_i,m}\right) + \left(\boldsymbol{u}_\mathrm{S}^{\mathbb{S},m+1} + \boldsymbol{\lambda}_\mathrm{S}^{\mathbb{S},m}\right)}{\sum_{i\in V_\mathrm{A}} 1 + 1} \tag{48}$$

where $\mathcal{E}_i$ is the set of all adjacent vehicle pairs that contain CAV i.

Step 4: The scaled dual variable $\boldsymbol{\lambda}$ is updated in each computing module:

$$\boldsymbol{\lambda}_i^{\mathbb{V}_i,m+1} = \boldsymbol{\lambda}_i^{\mathbb{V}_i,m} + \left(\boldsymbol{u}_i^{\mathbb{V}_i,m+1} - \boldsymbol{z}_i^{m+1}\right), \forall \boldsymbol{i} \in \boldsymbol{V_A} \tag{49}$$

$$\boldsymbol{\lambda}_i^{\mathbb{S},m+1} = \boldsymbol{\lambda}_i^{\mathbb{S},m} + \left(\boldsymbol{u}_i^{\mathbb{S},m+1} - \boldsymbol{z}_i^{m+1}\right), \forall \boldsymbol{i} \in \boldsymbol{V_A} \tag{50}$$

$$\boldsymbol{\lambda}_i^{\mathbb{R}_e,m+1} = \boldsymbol{\lambda}_i^{\mathbb{R}_e,m} + \left(\boldsymbol{u}_i^{\mathbb{R}_e,m+1} - \boldsymbol{z}_i^{m+1}\right), \quad \forall e \in \mathcal{E}, \forall i \in V_{\mathrm{A},e} \tag{51}$$

$$\boldsymbol{\lambda}_\boldsymbol{s}^{\mathbb{V}_i,m+1} = \boldsymbol{\lambda}_\boldsymbol{s}^{\mathbb{V}_i,m} + \left(\boldsymbol{u}_\boldsymbol{s}^{\mathbb{V}_i,m+1} - \boldsymbol{z}_\boldsymbol{s}^{m+1}\right), \forall \boldsymbol{i} \in \boldsymbol{V_A} \tag{52}$$

$$\boldsymbol{\lambda}_\mathrm{S}^{\mathbb{S},m+1} = \boldsymbol{\lambda}_\mathrm{S}^{\mathbb{S},m} + \left(\boldsymbol{u}_\mathrm{S}^{\mathbb{S},m+1} - \boldsymbol{z}_\mathrm{S}^{m+1}\right) \tag{53}$$

Step 5: Return to **Step 1** until the following stopping criterion is satisfied:

$$\left\|\boldsymbol{u}^{m+1} - \boldsymbol{z}^{m+1}\right\| \le \epsilon \tag{54}$$

where ϵ is the tolerance of the primal residual error.

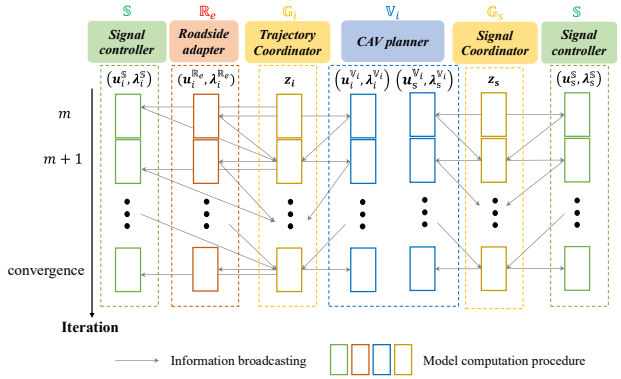

Fig. 4. The iteration process of the traditional ADMM algorithm for MVSC system.

The iteration process of the ADMM algorithm is illustrated in Fig. 4. . In each update, optimized solutions of signal controller $\mathbb{S}$, roadside adapter $\mathbb{R}_e$, and CAV planner $\mathbb{V}_i$ are given to their belonging coordinators ($\mathbb{G}_\mathrm{S}$ or $\mathbb{G}_i$). In the coordinator, consensus variables are generated for the computation of the next iteration. In each rolling step, HV trajectories are predicted based on the most recent CAV trajectories and signal plans from the previous iteration. As the ADMM iterations proceed, the discrepancy between successive solutions becomes smaller, making the predicted HV trajectories increasingly consistent with the current optimization results. This design ensures efficient cooperative decision-making in the mixed traffic environment.

2) Iteration schemes: Although the ADMM algorithm has guaranteed convergence ability to the global optimal for the convex problem, it still may require many iterations, especially in the multi-CAVs scenario [40]. In this paper, we propose two types of iteration schemes: complete iteration scheme and concomitant iteration scheme.

As shown in Fig. 5. (a), the complete iteration scheme is a generally adopted method which accomplishes the iteration and its convergence within each rolling [26], [41], [42]. For example, during rolling r, all subproblems need to be computed for M times to reach convergence. The complete iteration reboots in the next rolling or once the traffic environment is changed, such as when a new CAV drives into the scope. This kind of iteration scheme may be time-consuming and not ready for real-time computation. Furthermore, computation rebooting loses a lot of previous knowledge from the last iteration. It violates the reality that a light disturbance would not greatly change original strategies.

Therefore, we further propose a concomitant iteration scheme to enhance computation and convergence efficiency. The concomitant iteration scheme conducts iterations along with the rolling horizon execution. In this way, during each rolling, only one iteration is needed. Convergence is achieved with the increase of rolling execution in global time. Furthermore, the last iteration's knowledge is fully utilized as the input for the current iteration, in order to accelerate convergence and ensure resilience in the actual dynamic traffic environment.

The concomitant iteration scheme is illustrated Fig. 5. (b). During rolling r, the concomitant iteration scheme solves all subproblems based on consensus variables $\boldsymbol{z}$ and dual variables $\boldsymbol{\lambda}$ from last rolling $r-1$. It outputs control variables $\boldsymbol{u}_i^{\mathbb{V}_i}$ and $\boldsymbol{u}_\mathrm{S}^{\mathbb{S}}$ for CAVs and signal to execute. Consensus variables and dual variables are outputted for optimization in the next rolling.

In the proposed concomitant iteration scheme, the solutions executed at each rolling step may not have fully converged. There are two mechanisms that can ensure the executed decisions remain practically feasible. First, each CAV and the traffic signal execute the local optimization results (i.e., $\boldsymbol{u}_i^{\mathbb{V}_i}$ and $\boldsymbol{u}_\mathrm{S}^{\mathbb{S}}$) rather than the consensus variable optimization results $\boldsymbol{z}$. Even without full convergence, CAV controllers and the signal controller each solve their own subproblem subject to their respective feasibility constraints. As a result, the executed signal plan and CAV trajectories inherently comply with their individual operational and safety requirements. Second, each CAV is equipped with a lower-level trajectory tracking module (e.g., MPC) as shown in Fig. 5. , which takes the optimized trajectory from the proposed MVSC planner as a reference. The trajectory tracking module re-generates a feasible trajectory that strictly satisfies vehicle dynamics and safety constraints for execution [43]. This allows each CAV to adapt to its real-time state and maintain safety. Moreover, the proposed concomitant iteration operates in short rolling

horizons, enabling rapid correction in subsequent steps. By fully leveraging the previous iteration's knowledge, convergence is achieved as the number of rolling executions increases over global time.

V. Evaluations

The proposed MVSC controller is evaluated from the following aspects: i) function validation; ii) mobility; iii) ecology; and iv) computational efficiency.

A. Experiment Design

The simulation is implemented in SUMO (Simulation of Urban MObility) [44]. CAVs and traffic signal in SUMO are controlled through the interface *TraCI* in Python 3.11 with *Gurobi* as a solver. The simulation experiment runs on a laptop with an Intel i9-13900H processor at 3.4 GHz and 32 GB of RAM. The delay in communications is assumed to be negligible. Each simulation lasted 1800s with a warm-up period of 150s.

The proposed method is implemented in a typical four-arm intersection scenario, as shown in Fig. 1. (a). Each arm includes three lanes, assigned to left-turn, through, and right-turn movements, respectively. Although each movement is assigned to a dedicated lane in this study, the proposed model is still applicable in cases with shared lanes. Under the lane-based signal optimization framework, movements sharing the same lane are typically grouped into the same signal phase [45]. Therefore, the proposed model and algorithm are applicable to other intersection configurations with shared lanes. In the experiment intersection, right-turn vehicles have no conflicts with through and left-turning vehicles from other arms. Therefore, they will not be controlled by the signal in this study. The right-turning movements are continuously granted green time in this study. Note that our proposed model is still applicable in the case that the traffic light should control the right-turning movement, in which case the decision variables of right-turn phases and CAVs can be included.

The ideal communication environment assumption is adopted in this study. In practical deployments, however, communication delays and packet losses may occur. Under such conditions, our framework can be extended by incorporating delay-tolerant prediction and state estimation modules to replace missing or outdated variables [46].

TABLE I shows the benchmark traffic demand. The volume/capacity (V/C) ratio is 0.5. The capacity is calculated as reference [27]. This study evaluates the proposed planner under four traffic demand levels, with V/C ratios set as 0.5, 0.75, 1.0, and 1.25. Four CAV penetration rates (i.e., 20%, 40%, 60%, and 80%) are considered to evaluate the effectiveness of the cooperative decision-making model and parallel algorithm. The V/C ratio and CAV penetration rate are initially set as 0.5 and 40% respectively, except in the sensitivity analysis.

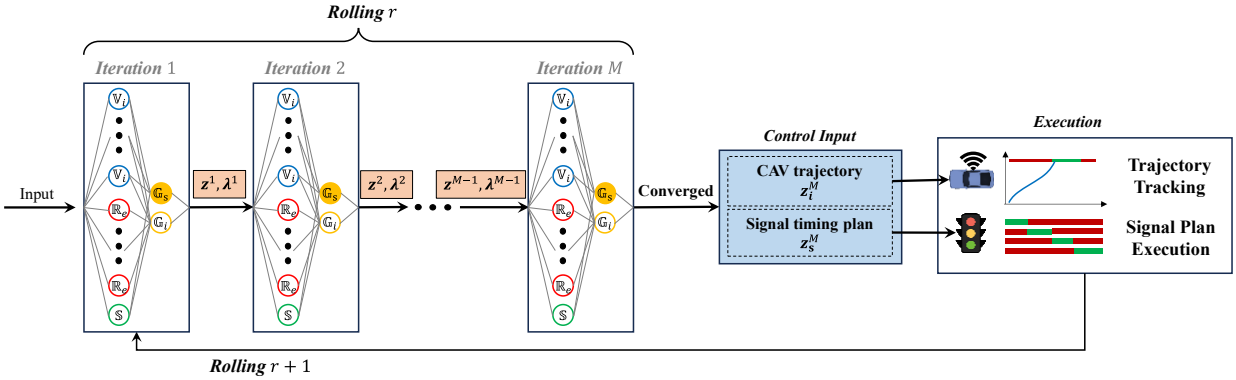

(a) Complete iteration scheme (within a rolling)

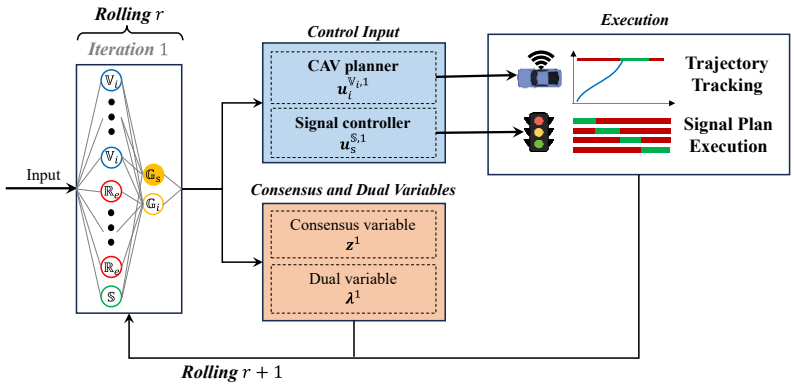

(b) Concomitant iteration scheme (with rollings)

Fig. 5. The diagram of complete iteration and concomitant iteration schemes.

TABLE I
BENCHMARK TRAFFIC DEMAND OF EVALUATION

Traffic demand (V/C)	To arm			
From arm	E	N	W	S
E	--	1200 pcu/h (0.5)	270 pcu/h (0.5)	270 pcu/h (0.5)
N	270 pcu/h (0.5)	--	1200 pcu/h (0.5)	270 pcu/h (0.5)
W	270 pcu/h (0.5)	270 pcu/h (0.5)	--	1200 pcu/h (0.5)
S	1200 pcu/h (0.5)	270 pcu/h (0.5)	270 pcu/h (0.5)	--

B. Control Methods

In our experiment, the performance and effectiveness of the proposed controller are evaluated in comparison with current-widely used actuated signal controller:

- **The proposed MVSC controller:** The proposed MVSC controller plans all CAVs' trajectories and optimizes signal timing at the same time.
- **Baseline (Actuated signal controller):** It is a widely used signal control method. It decides whether to extend or terminate the current green duration in response to the real-time traffic state. The minimum green time and maximum green time for each phase are 10s and 50s, respectively. The max gap, detector gap, and passing time are set as 3s, 2s, and 2s, respectively.

Moreover, the proposed two iteration schemes, complete iteration and concomitant iteration, are tested to verify their computational efficiency.

C. Parameter Setting

The following settings are adopted.

- Free flow speed: 13.89m/s (i.e., 50 km/h)
- The maximum speed $v_{\max}$: 16.67m/s (i.e., 60 km/h)
- The minimum acceleration $a_{\min}$: -3m/s2
- The maximum acceleration $a_{\max}$: 3m/s2
- Safety headway t_{safe}: 2s
- The minimum and maximum green time $g_{\min}$ and $g_{\max}$: 10s and 50s [47]
- The minimum and maximum cycle length $C_{\min}$ and $C_{\max}$: 60s and 150s
- The loss time and inter-green time l: 3s
- Weight factors α_1, α_2, β_1, β_2, and β_3: 0.5, 0.5, 1, 1, and 10
- Penalty parameter ρ: 200
- Tolerance of stopping criterion ϵ: 0.1
- Maximum iteration in complete iteration scheme: 200
- Rolling step interval: 0.02s
- IDM parameters are set as reference [38]

D. Measure of Effectiveness

Measures of Effectiveness (MOEs) are as follows.

- *Function validation*: To verify the function of jointly optimizing signal timing and CAVs' trajectories, the trajectories of both CAVs and HVs are analyzed.
- *Mobility*: This MOE is quantified from the following aspects: 1) average delay; 2) average number of stops.
- *Ecology*: This MOE is quantified by the average fuel consumption and CO2 emission. The emission model in the report of the US Environmental Protection Agency (EPA) is applied for the estimation of consumption and emission [48].
- *Computational efficiency*: It is quantified by the iteration times before convergence and solution time.

E. Experiment Results

Results demonstrate that compared to the conventional actuated signal controller, the proposed MVSC method is capable of: i) joint planning multi-CAVs' trajectories and signal timing; ii) enhancing CAVs' mobility by 8.48% and ecology by 3.78% compared to HVs; iii) enhancing global traffic mobility by 23.60% and ecology by 15.63%. Furthermore, the computational efficiency of the proposed two iteration schemes is evaluated. Results show that concomitant iteration enables: i) average solution time within 10 milliseconds, which is 1/157 of complete iteration; ii) 42.86% of convergence efficiency in the dynamic traffic environment.

1) Function validation:

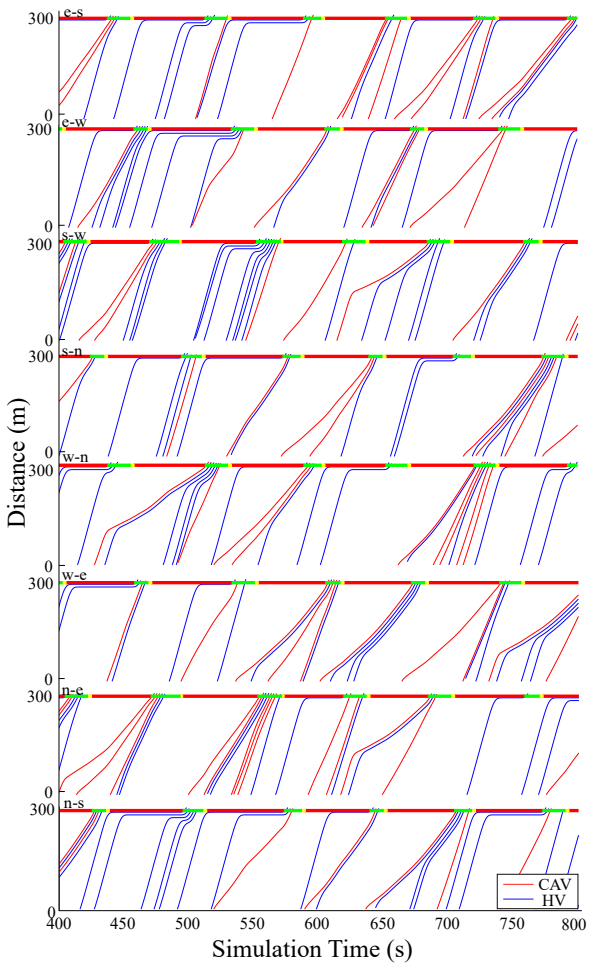

Fig. 6. Trajectories of CAVs and HVs and signal plan.

The function of jointly optimizing signal timing plan and multi-CAVs' trajectories is validated in Fig. 6. It shows that the proposed planner can adjust signal timing according to traffic conditions to minimize global delay. As shown in Fig. 6, the phase duration is unfixed and can adapt to the time-

varying traffic. At the same time, CAVs can dynamically adjust trajectory (decelerate or accelerate) to catch up with the green duration. The proposed planner is verified to be capable of cooperative decision-making among multiple CAVs. As shown in Fig. 6, seventy-eight CAVs in an intersection are tested within 400 seconds. The proposed planner computes each CAV's trajectory. The planned trajectory enables CAV to pass the intersection without stops and collisions. Moreover, CAVs can affect following HVs and lead them to also pass the intersection smoothly. If the HV is not led by a CAV, it may have to stop and wait at the stop line, which brings additional fuel consumption and emission. Hence, the proposed MVSC planner is demonstrated to improve global traffic efficiency and ecology at the intersection.

The observed differences in CAV deceleration patterns in Fig. 6 stem from the flexibility of the joint optimization framework. CAVs that are farther from the stop line may start decelerating earlier and more gradually if the controller determines they are unlikely to pass during the current green phase. Conversely, CAVs closer to the intersection may decelerate more sharply when the signal phase is no longer reachable. In addition, the MVSC planner considers system-level objectives such as reducing overall delay or leading HVs through the intersection. As a result, CAVs may adjust their trajectories not solely for their own mobility but to improve overall efficiency, leading to diverse deceleration behaviors.

2) CAVs' mobility and ecology: TABLE II shows the comparison of the mobility and ecology performance for both CAVs and HVs in the four-arm intersection scenario. Compared to HVs, the proposed MVSC controller is capable of enhancing CAVs' mobility by 8.48%, via reducing the number of stops and further reducing loss time from start-up. The CAVs' ecology could also be enhanced by 3.78%, due to a more ecological trajectory.

TABLE II
CAVS' PERFORMANCE COMPARED TO HVS.

	Average delay (s/veh)	Average number of stops	Average Fuel Consumption (g/veh)	Average CO2 emissions (g/veh)
CAVs	30.44	0.00	58.11	182.20
HVs	33.26	0.39	60.40	189.36

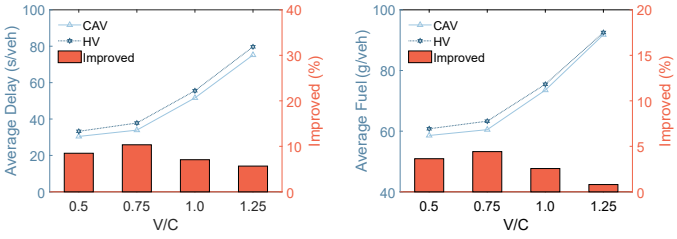

(a) Mobility performance (b) Ecology performance

Fig. 7. Sensitivity analysis under different V/C ratios for CAVs and HVs.

To further analyze the benefits of CAVs in our MVSC controller, we conduct a sensitivity analysis for CAVs and HVs under different V/C ratios in the four-arm intersection scenario. As shown in Fig. 7. (a) and (b), CAVs' and HVs' delay and fuel consumption would increase with the increase of traffic density, since more congested traffic always leads to queuing before the stop line. No matter the traffic density, the proposed MVSC controller could always reduce drive delay and fuel consumption. However, the performance enhancement reaches the highest value at V/C of 0.75. It makes sense that the proposed MVSC controller could ensure driving mobility and ecology which is insensitive to traffic density. Compared to the great increase in conventional HVs' delay and fuel consumption from V/C=0.5 to V/C=0.75, the mobility and ecology of the proposed MVSC controller would not deteriorate a lot. Hence, performance enhancement would increase from V/C=0.5 to V/C=0.75. However, in congested traffic, like V/C greater than 1.0, the proposed MVSC controller cannot make a great difference either. Its performance enhancement would reduce when V/C is greater than 0.75.

3) Global traffic mobility and ecology: TABLE III shows the comparison of the global mobility and ecology performance between the proposed MVSC controller and the baseline actuated signal controller in the four-arm intersection scenario. Results show that the proposed MVSC controller can significantly reduce travel delay by 23.60% and reduce the number of stops by 77.42%. Due to remarkably eliminated stop-and-go maneuvers, the proposed MVSC controller reduces fuel consumption and CO_2 emission by 15.63%. Hence, the proposed MVSC controller is demonstrated with enhancing global traffic mobility and ecology.

TABLE III
GLOBAL TRAFFIC PERFORMANCE COMPARISON.

	Average delay (s/veh)	Average number of stops	Average Fuel Consumption (g/veh)	Average CO2 emissions (g/veh)
Baseline	38.98	0.93	70.58	221.28
Proposed	29.78	0.21	59.55	186.70

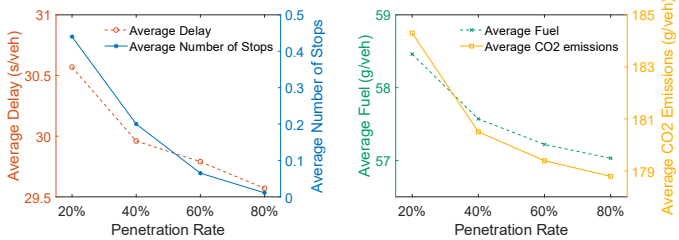

(a) Mobility performance (b) Ecology performance

Fig. 8. Sensitivity analysis under different CAV penetration rates for the proposed MVSC controller.

A sensitivity analysis is conducted for global traffic mobility and ecology in regard to CAV penetration rate, as shown in Fig. 8. As shown in Fig. 8. (a), the proposed MVSC controller enhances global traffic mobility with the increase in CAV penetration rate. As shown in Fig. 8. (b), the proposed MVSC controller also enhances global traffic ecology with the increase of CAV penetration rates. It makes sense since more CAVs can better lead HVs to pass the intersection smoothly.

This article has been accepted for publication in IEEE Internet of Things Journal. This is the author's version which has not been fully edited and content may change prior to final publication. Citation information: DOI 10.1109/JIOT.2025.3610639

This impact has been verified by Fig. 9. It shows that the distribution of the HVs' delay and fuel consumption shows a greater skewness towards the lower value with the increase of CAV's penetration rate. Furthermore, an interesting finding is that the marginal reductions are largest when the penetration rate increases from 20% to 40% for both mobility and ecology, as shown in Fig. 8. The marginal benefit becomes less significant for further penetration rate increasement. It reveals that in the implementation of CAV technology, we do not need to pursue a high penetration rate. With the hand of the proposed MVSC method, we can receive a significant reward for traffic mobility and ecology at a CAV penetration rate of 40%.

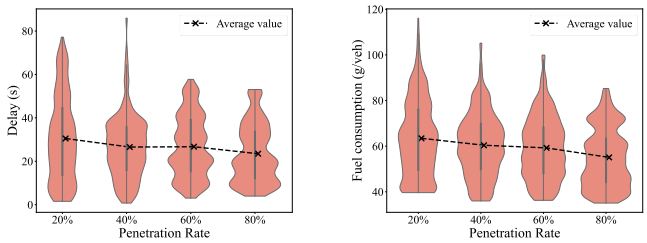

(a) HVs' mobility performance (b) HVs' ecology performance

Fig. 9. Impacts on HVs' mobility and ecology at different CAV penetration rates.

We further conduct a sensitivity analysis across various traffic densities, ranging from under-saturated (V/C=0.5) to over-saturated (V/C=1.25). As shown in Fig. 10. (a) and (b), global traffic mobility and ecology deteriorate with the increase in traffic density. However, our proposed MVSC controller enhances global traffic mobility and ecology, regardless of the traffic density. The performance enhancement of our proposed method varies with traffic density. Notably, at V/C=0.75, our method demonstrates the most substantial improvements in both traffic mobility and sustainability, indicating a 28.58% reduction in average delay and a 20.35% reduction in average fuel consumption. It is because the proposed controller can maneuver CAVs to lead more HVs, to fully utilize temporal and spatial road resources by ecologically catching up green light, when V/C increases from 0.5 to 0.75. Nevertheless, when the V/C ratio is greater than 0.75, traffic is too congested and CAVs also have to wait for passing opportunities. In this case, CAVs still show their guidance effect on HVs, while not as impressive as the scenario of non-congested traffic.

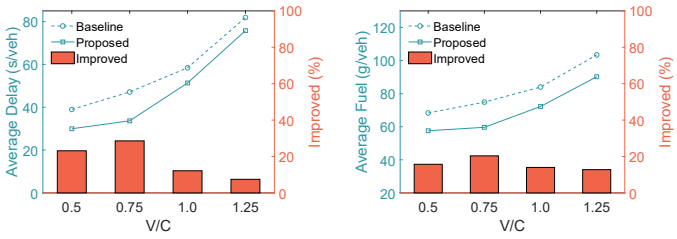

(a) Mobility performance (b) Ecology performance

Fig. 10. Sensitivity analysis under different V/C ratios for the proposed MVSC controller.

4) Computational efficiency:

a) Convergence performance: We firstly test the convergence of both complete and concomitant iteration schemes in a sampled scenario with 8 CAVs for clarity. The comprehensive evaluation in solution time in real traffic scenario will be detailed in the next section.

Fig. 11 shows the primal errors of these 8 CAVs' control variables. The decrease in primal residuals indicates that the consensus variables and control variables become closer to each other. In this situation, the complete iteration scheme needs 30 times of iterations within one rolling to converge. As shown in Fig. 11. (b), the concomitant iteration scheme converges within 37 times of iterations. It makes sense since the execution error exists when iterating along with rolling updating.

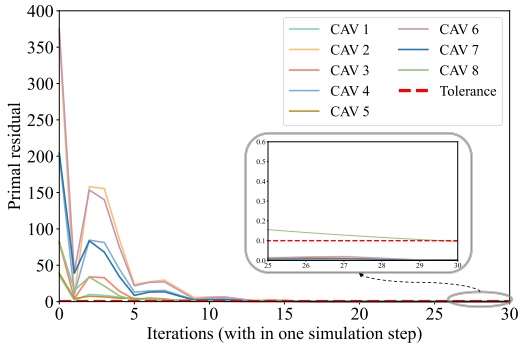

(a) Complete iteration

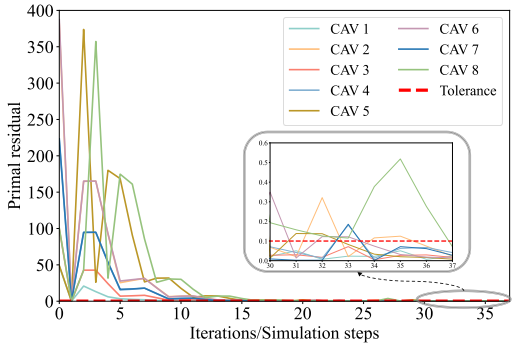

(b) Concomitant iteration

Fig. 11. Convergence performance of complete and concomitant iteration scheme.

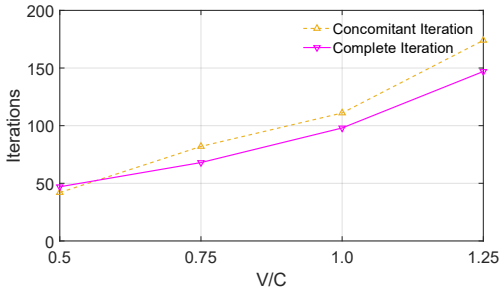

Fig. 12. Convergence performance under different V/C ratios.

We further conduct a sensitivity analysis of convergence performance under different V/C ratios. As shown in Fig. 12. ,

This article has been accepted for publication in IEEE Internet of Things Journal. This is the author's version which has not been fully edited and content may change prior to final publication. Citation information: DOI 10.1109/JIOT.2025.3610639

both complete and concomitant iteration schemes need more iterations with the increase of traffic density. When there are more vehicles in the intersection scope, more variables need to be coordinated in the MVSC planner. As a result, it needs more iterations to find the optimal result. The concomitant iteration scheme sacrifices 13.61% convergence performance compared to the complete iteration scheme on average in Fig. 12. . However, this sacrifice is acceptable, considering only one iteration within each rolling would greatly enhance computational efficiency, which would be discussed in the next section.

Furthermore, we have verified the convergence resilience of the concomitant iteration scheme in the dynamic traffic environment in this sampled scenario. As shown in Fig. 13. , two new vehicles (CAV 9 and CAV 10) drive into the cooperation region at simulation time 2. In this case, the concomitant iteration scheme does not have to reboot for a new calculation. Consensus variables from the last planning could be inputted as the prior knowledge, which greatly conforms to the reality that a light disturbance would not greatly change the original strategy. Hence, in the new calculation, the concomitant iteration scheme only needs 40 iterations (i.e., 0.8 seconds), as shown in Fig. 13 (a). The convergence efficiency shows an enhancement of 42.86% compared to the complete iteration scheme in this sampled scenario, as shown in Fig. 13 (b) (70 iterations in the complete iteration scheme). Therefore, in real-world dynamic environment, the proposed MVSC planner would swiftly recover to the convergence level, highlighting the concomitant iteration algorithm's resilience in implementations.

Moreover, as shown in both Fig. 11 and Fig. 13, concomitant iteration scheme exhibits stronger oscillations compared to the complete iteration scheme. It is because the concomitant iteration scheme performs only one ADMM update per rolling step, while the traffic state changes between steps. Each step is warm-started by the previous solution, but after execution the realized system state deviates slightly from the prediction, introducing larger execution error. However, by limiting each rolling window to a single update, the computation time per step is significantly reduced, enabling real-time implementation. These oscillations tend to diminish over successive steps as the algorithm tracks the moving optimum, ensuring stable system performance in practice.

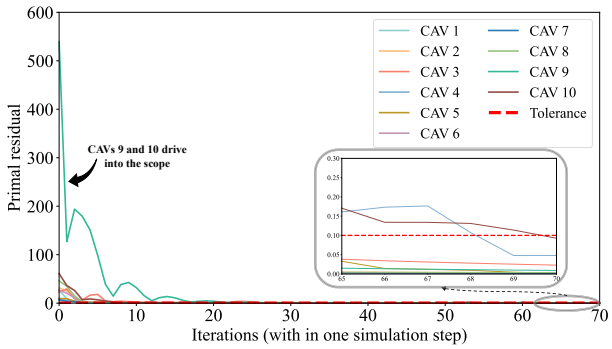

(a) Complete iteration

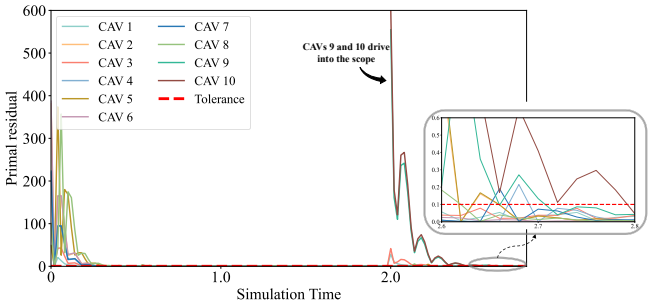

(b) Concomitant iteration

Fig. 13. Convergence resilience when new CAVs drive into the intersection scope.

b) Solution time: Based on the convergence performance evaluation in the sampled scenario, we further conduct a comprehensive assessment of solution times in real traffic conditions. The evaluation results highlight the benefits of concomitant iteration scheme from conducting one iteration within each rolling.

The sensitivity analysis on solution time under varying V/C ratios is conducted in regard to traffic density for the concomitant iteration scheme and complete iteration scheme. Fig. 14 shows that the concomitant iteration scheme significantly enhances computational efficiency. Compared to the complete iteration scheme, the concomitant iteration scheme only calls for 1/157 of solution time on average. Specifically, as shown in Fig. 14, the complete iteration scheme shows an increasing solution time with the increase of traffic density. In congested traffic (i.e., V/C ratio is greater than 1), the average solution time of complete iteration is greater than one second. It is because when more CAVs are included in the planning, more variables are introduced into coordinators, which calls for a significantly increasing number of iterations. Real-time implementation may be infeasible. Comparably, the concomitant iteration scheme shows a robust computational efficiency against various V/C ratios, since it only has to conduct one iteration within a rolling. The average solution time is always under 10 milliseconds. It indicates that the proposed MVSC planner is enabled to be implemented in real time. Considering the 1/157 of solution time in each rolling, the concomitant iteration scheme's 13.61% convergence performance sacrifice is acceptable.

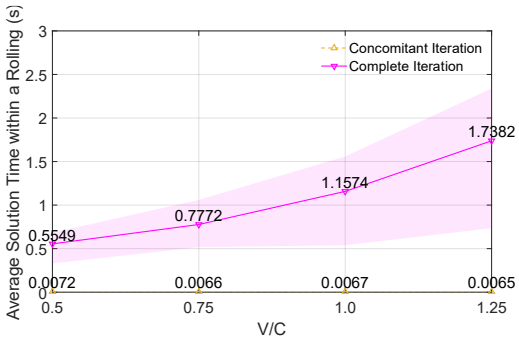

Fig. 14. Average solution time of complete and concomitant iteration schemes within a rolling.

Experimental results show that the concomitant iteration requires significantly less computation time per rolling step compared to the complete iteration, enabling real-time execution. Although only the one-rolling optimization results are executed, the warm-start mechanism in the concomitant iteration scheme allows the algorithm to rapidly reduce the optimality gap in subsequent iterations. As a result, the overall solution trajectory converges toward the optimum over global time, achieving long-term performance close to that of the complete iteration while maintaining substantially lower computational cost.

VI. Conclusion and Future Research

This research proposes a Multi-Vehicles and Signal Coordination (MVSC) controller within the context of IoT. It enables joint optimization of all CAVs' trajectories and signal plan via formulating in the spatial domain. The centralized problem is decomposed into several subproblems and solved by a parallel computing approach. We perform simulation experiments to evaluate the performance of the MVSC controller. Results show that:

- The proposed MVSC functions as expected and is capable of coordinating multi-CAVs' trajectories and traffic signal timing.
- The proposed controller can reduce the CAVs' delay by 8.48% and fuel consumption by 3.78% compared to HVs.
- The proposed MVSC controller is verified to utilize CAVs to lead HVs to pass the intersection smoothly. It enhances global traffic mobility by 23.60% and ecology by 15.63%.
- The proposed MVSC controller has better performance at different CAV penetration rates and V/C ratios. CAV's penetration rate of 40% has the largest reward for traffic mobility and ecology. The V/C ratio of 0.75 shows the greatest performance enhancement.
- The proposed concomitant iteration scheme only needs less than 10 milliseconds of computation time, which is 1/157 of the solution time of the complete iteration scheme. This significant enhancement in computational efficiency stands on only 13.61% of sacrifice on convergence.
- The concomitant iteration scheme has better convergence resilience in the dynamic traffic environment. It enhances convergence efficiency by 42.86% compared to the complete iteration scheme.

This research opens several interesting directions for future work. First, future research efforts could focus on extending the planner to consider lane-changing behaviors. Extending the framework to account for lane-changing behaviors requires two-dimensional spatial modeling. It substantially increases the complexity of vehicle dynamics and collision constraints. Second, we will generalize the proposed cooperative decision-making problem at the isolated intersection to multiple coordinated intersections for urban arterial or urban networks in our future works. Third, future research should explicitly consider communication delays and even packet losses in the information exchange, thereby enhancing its applicability and reliability in real-world IoT environments.

Appendix

The main variables are listed below:

Variable	
$a_{i,k}$	Acceleration of vehicle i at space step k
$t_{i,k}$	Arrival time of vehicle i at space step k
$\pi_{i,k}$	Reciprocal of the speed of vehicle i at space step k
$t_p^{\mathrm{b}}, t_p^{\mathrm{e}}$	Beginning and ending time of green duration of phase p
C	Signal cycle length
$\boldsymbol{u}_i$	Vehicle control variable vector
$\boldsymbol{u}_{\mathrm{s}}$	Signal control variable vector
$\boldsymbol{z}_i, \boldsymbol{z}_{\mathrm{s}}$	Consensus variable of vehicle i and signal
$\boldsymbol{\lambda}$	Scaled dual variable
Sets	
V	Set of all vehicles
V_{A}	Set of all CAVs
V_{H}	Set of all HVs
$\mathcal{E}$	Set of all pairwise adjacent vehicles
$V_{\mathrm{A},e}$	Set of CAVs corresponding to the adjacent vehicles pair $e \in \mathcal{E}$
P	Set of all phases of the signal plan
Parameters	
$v_{\max}$	Maximum speed
$a_{\min}, a_{\max}$	Minimum and maximum acceleration
t_{safe}	Safety headway
$g_{\min}, g_{\max}$	Minimum and maximum green time
$C_{\min}, C_{\max}$	Minimum and maximum cycle length
ρ	Penalty parameter in the ADMM

References

[1] Noc. ITE, *Traffic Signal Benchmarking and State of the Practice Report [Internet]. 2020*. 2019.

[2] H. Xia *et al.*, "Field operational testing of eco-approach technology at a fixed-time signalized intersection," in *2012 15th International IEEE Conference on Intelligent Transportation Systems*, IEEE, 2012, pp. 188–193.

[3] B. Gao, J. Liu, H. Zou, J. Chen, L. He, and K. Li, "Vehicle-Road-Cloud Collaborative Perception Framework and Key Technologies: A Review," *IEEE Transactions on Intelligent Transportation Systems*, 2024, Accessed: Dec. 25, 2024. [Online]. Available: https://ieeexplore.ieee.org/abstract/document/10700687/

[4] L. F. P. De Oliveira, L. T. Manera, and P. D. G. Da Luz, "Development of a smart traffic light control system with real-time monitoring," *IEEE Internet of Things Journal*, vol. 8, no. 5, pp. 3384–3393, 2020.

[5] J. Hu, S. Li, H. Wang, Z. Wang, and M. J. Barth, "Eco-approach at an isolated actuated signalized intersection: Aware of the passing time window," *Journal of Cleaner Production*, vol. 435, p. 140493, Jan. 2024, doi: 10.1016/j.jclepro.2023.140493.

[6] C. Ma, C. Yu, and X. Yang, "Trajectory planning for connected and automated vehicles at isolated signalized intersections under mixed traffic environment," *Transportation research part C: emerging technologies*, vol. 130, p. 103309, 2021.

[7] J. Zhu, C. Ma, Y. Shi, Y. Yang, Y. Guo, and X. Yang, "Asynchronous decentralized traffic signal coordinated control in urban road network," *Computer aided Civil Eng*, vol. 40, no. 7, pp. 895–916, Mar. 2025, doi: 10.1111/mice.13362.

[8] Y. Du, W. ShangGuan, and L. Chai, "A coupled vehicle-signal control method at signalized intersections in mixed traffic environment," *IEEE Transactions on Vehicular Technology*, vol. 70, no. 3, pp. 2089–2100, 2021.

[9] M. Tajalli and A. Hajbabaie, "Traffic Signal Timing and Trajectory Optimization in a Mixed Autonomy Traffic Stream," *IEEE Trans. Intell. Transport. Syst.*, vol. 23, no. 7, pp. 6525–6538, Jul. 2022, doi: 10.1109/TITS.2021.3058193.

[10] J. Hu, Y. Feng, X. Li, and H. Wang, "A Model Predictive Control Based Path Tracker in Mixed-Domain," in *2021 IEEE Intelligent Vehicles Symposium (IV)*, IEEE, 2021, pp. 1255–1260.

[11] Z. Yao, B. Zhao, T. Yuan, H. Jiang, and Y. Jiang, "Reducing gasoline consumption in mixed connected automated vehicles environment: A joint optimization framework for traffic signals and vehicle trajectory," *Journal of cleaner production*, vol. 265, p. 121836, 2020.

[12] B. Xu *et al.*, "Cooperative method of traffic signal optimization and speed control of connected vehicles at isolated intersections," *IEEE Transactions on Intelligent Transportation Systems*, vol. 20, no. 4, pp. 1390–1403, 2018.

[13] K. Yang, S. I. Guler, and M. Menendez, "Isolated intersection control for various levels of vehicle technology: Conventional, connected, and automated vehicles," *Transportation Research Part C: Emerging Technologies*, vol. 72, pp. 109–129, Nov. 2016, doi: 10.1016/j.trc.2016.08.009.

[14] M. Liu, J. Zhao, S. Hoogendoorn, and M. Wang, "A single-layer approach for joint optimization of traffic signals and cooperative vehicle trajectories at isolated intersections," *Transportation Research Part C: Emerging Technologies*, vol. 134, p. 103459, Jan. 2022, doi: 10.1016/j.trc.2021.103459.

[15] H. Wang, W. Hao, J. So, Z. Chen, and J. Hu, "A Faster Cooperative Lane Change Controller Enabled by Formulating in Spatial Domain," *IEEE Trans. Intell. Veh.*, vol. 8, no. 12, pp. 4685–4695, Dec. 2023, doi: 10.1109/TIV.2023.3317957.

[16] H. Wang, J. Lai, X. Zhang, Y. Zhou, S. Li, and J. Hu, "Make space to change lane: A cooperative adaptive cruise control lane change controller," *Transportation research part C: emerging technologies*, vol. 143, p. 103847, 2022.

[17] F. Tian *et al.*, "Trajectory planning for autonomous mining trucks considering terrain constraints," *IEEE Transactions on Intelligent Vehicles*, vol. 6, no. 4, pp. 772–786, 2021.

[18] S. Li, H. Wang, and J. Hu, "Ecological driving at an actuated signalized intersection: A practical solution of Vehicle-Road-Cloud Integration system," *Transportation Research Part C: Emerging Technologies*, vol. 177, p. 105198, 2025.

[19] S. M. A. B. A. Islam and A. Hajbabaie, "Joint Signal Timing and Trajectory Control With Uncertainty in Connected Automated Vehicle Dynamics," *IEEE Trans. Intell. Transport. Syst.*, pp. 1–13, 2024, doi: 10.1109/TITS.2024.3389818.

[20] A. Mirheli, L. Hajibabai, and A. Hajbabaie, "Development of a signal-head-free intersection control logic in a fully connected and autonomous vehicle environment," *Transportation Research Part C: Emerging Technologies*, vol. 92, pp. 412–425, 2018.

[21] R. Niroumand, L. Hajibabai, and A. Hajbabaie, "Advancing the white phase mobile traffic control paradigm to consider pedestrians," *Computer aided Civil Eng*, vol. 39, no. 13, pp. 1946–1962, Jul. 2024, doi: 10.1111/mice.13178.

[22] Q. Liu, K. Zhang, M. Li, X. Chen, X. Lin, and S. Li, "Integrated optimization of traffic signal timings and vehicle trajectories considering mandatory lane-changing at isolated intersections," *Transportation Research Part C: Emerging Technologies*, vol. 163, p. 104614, 2024.

[23] Y. Xu, Y. Shi, X. Tong, S. Chen, and Y. Ge, "A Multi-agent Reinforcement Learning Based Control Method for Connected and Autonomous Vehicles in A Mixed Platoon," *IEEE Transactions on Vehicular Technology*, 2024, Accessed: Jan. 27, 2025. [Online]. Available: https://ieeexplore.ieee.org/abstract/document/10561539/

[24] Y. Gu, L. Wang, L. Cheng, and G. Gu, "An IoT-Based Framework for Motion Planning of Connected Automated Vehicles at Signal-Free Traffic Intersections," *IEEE Internet of Things Journal*, vol. 11, no. 22, pp. 35752–35761, 2023.

[25] J. Shen, E. K. H. Kammara, and L. Du, "Nonconvex, fully distributed optimization based CAV platooning control under nonlinear vehicle dynamics," *IEEE Transactions on Intelligent Transportation Systems*, vol. 23, no. 11, pp. 20506–20521, 2022.

[26] S. E. Li *et al.*, "Synchronous and asynchronous parallel computation for large-scale optimal control of connected vehicles," *Transportation Research Part C: Emerging Technologies*, vol. 121, p. 102842, Dec. 2020, doi: 10.1016/j.trc.2020.102842.

[27] C. Ma, C. Yu, C. Zhang, and X. Yang, "Signal timing at an isolated intersection under mixed traffic environment with self-organizing connected and automated vehicles," *Computer aided Civil Eng*, vol. 38, no. 14, pp. 1955–1972, Sep. 2023, doi: 10.1111/mice.12961.

[28] D. Li, A. Liu, H. Pan, and W. Chen, "Safe, Efficient and Socially-Compatible Decision of Automated Vehicles: A Case Study of Unsignalized Intersection Driving," *Automot. Innov.*, vol. 6, no. 2, pp. 281–296, May 2023, doi: 10.1007/s42154-023-00219-2.

[29] C. Yu, W. Sun, H. X. Liu, and X. Yang, "Managing connected and automated vehicles at isolated intersections: From reservation-to optimization-based methods," *Transportation research part B: methodological*, vol. 122, pp. 416–435, 2019.

[30] J. Zhao, T. Yao, C. Zhang, and M. A. Shafique, "Signal control for overflow prevention at intersections using partial connected vehicle data," *Transportmetrica A: Transport Science*, pp. 1–31, Jun. 2024, doi: 10.1080/23249935.2024.2361648.

[31] Y. Feng, C. Yu, and H. X. Liu, "Spatiotemporal intersection control in a connected and automated vehicle environment," *Transportation Research Part C: Emerging Technologies*, vol. 89, pp. 364–383, Apr. 2018, doi: 10.1016/j.trc.2018.02.001.

[32] J. Hu *et al.*, "Vehicles Swarm Intelligence: Cooperation in both Longitudinal and Lateral Dimensions," *IEEE Transactions on Intelligent Vehicles*, 2024, Accessed: Jul. 01, 2024. [Online]. Available: https://ieeexplore.ieee.org/abstract/document/10553311/

[33] C. Yu, Y. Feng, H. X. Liu, W. Ma, and X. Yang, "Integrated optimization of traffic signals and vehicle trajectories at isolated urban intersections," *Transportation Research Part B: Methodological*, vol. 112, pp. 89–112, Jun. 2018, doi: 10.1016/j.trb.2018.04.007.

[34] H. Dui, S. Zhang, M. Liu, X. Dong, and G. Bai, "IoT-enabled real-time traffic monitoring and control management for intelligent transportation systems," *IEEE Internet of Things Journal*, vol. 11, no. 9, pp. 15842–15854, 2024.

[35] J. Hu, S. Luo, J. Lai, and C. Liu, "Enhanced Infrastructure Enabled Perception System Based on Edge Computing," *IEEE Internet of Things Journal*, 2025, Accessed: Jun. 17, 2025. [Online]. Available: https://ieeexplore.ieee.org/abstract/document/10855548/

[36] M. Lei, H. Wang, D. Li, Z. Li, A. Dhamaniya, and J. Hu, "Space Domain based Ecological Cooperative and Adaptive Cruise Control on Rolling Terrain," May 13, 2024, *arXiv*: arXiv:2405.07553. Accessed: Jul. 01, 2024. [Online]. Available: http://arxiv.org/abs/2405.07553

[37] H. Zheng, R. R. Negenborn, and G. Lodewijks, "Fast ADMM for Distributed Model Predictive Control of Cooperative Waterborne AGVs," *IEEE Trans. Contr. Syst. Technol.*, vol. 25, no. 4, pp. 1406–1413, Jul. 2017, doi: 10.1109/TCST.2016.2599485.

[38] M. Treiber, A. Hennecke, and D. Helbing, "Congested traffic states in empirical observations and microscopic simulations," *Physical review E*, vol. 62, no. 2, p. 1805, 2000.

[39] S. Boyd, N. Parikh, E. Chu, B. Peleato, and J. Eckstein, "Distributed optimization and statistical learning via the alternating direction method of multipliers," *Foundations and Trends® in Machine learning*, vol. 3, no. 1, pp. 1–122, 2011.

[40] T.-H. Chang, M. Hong, W.-C. Liao, and X. Wang, "Asynchronous distributed ADMM for large-scale optimization—Part I: Algorithm and convergence analysis," *IEEE Transactions on Signal Processing*, vol. 64, no. 12, pp. 3118–3130, 2016.

[41] X. Zhang, Z. Cheng, J. Ma, S. Huang, F. L. Lewis, and T. H. Lee, "Semi-Definite Relaxation-Based ADMM for Cooperative Planning and Control of Connected Autonomous Vehicles," *IEEE Trans. Intell. Transport. Syst.*, vol. 23, no. 7, pp. 9240–9251, Jul. 2022, doi: 10.1109/TITS.2021.3094215.

[42] Z. Huang, S. Shen, and J. Ma, "Decentralized iLQR for cooperative trajectory planning of connected autonomous vehicles via dual consensus ADMM," *IEEE Transactions on Intelligent Transportation Systems*, 2023, Accessed: Oct. 14, 2024. [Online]. Available: https://ieeexplore.ieee.org/abstract/document/10171831/

[43] C. Huang *et al.*, "Personalized Trajectory Planning and Control of Lane-Change Maneuvers for Autonomous Driving," *IEEE Trans. Veh. Technol.*, vol. 70, no. 6, pp. 5511–5523, Jun. 2021, doi: 10.1109/TVT.2021.3076473.

[44] P. A. Lopez *et al.*, "Microscopic traffic simulation using sumo," in *2018 21st international conference on intelligent transportation systems (ITSC)*, IEEE, 2018, pp. 2575–2582. Accessed: Jun. 16, 2024. [Online]. Available: https://ieeexplore.ieee.org/abstract/document/8569938/

[45] C. K. Wong and S. C. Wong, "Lane-based optimization of signal timings for isolated junctions," *Transportation Research Part B: Methodological*, vol. 37, no. 1, pp. 63–84, Jan. 2003, doi: 10.1016/S0191-2615(01)00045-5.

[46] D. Rong, S. Jin, and C. Yang, "Connected and autonomous vehicle trajectory planning considering communication delay," *IEEE Transactions on Vehicular Technology*, vol. 73, no. 9, pp. 12668–12681, 2024.

[47] P. Koonce, "Traffic signal timing manual," United States. Federal Highway Administration, 2008. Accessed: Dec. 26, 2024. [Online]. Available: https://rosap.ntl.bts.gov/view/dot/800

[48] H. C. Frey, A. Unal, J. Chen, S. Li, and C. Xuan, "Methodology for developing modal emission rates for EPA's multi-scale motor vehicle & equipment emission system," *Ann Arbor, Michigan: US Environmental Protection Agency*, p. 13, 2002.

Jichen Zhu received the B.S. degree in transportation engineering from Central South University, Changsha, China, in 2020. He is currently pursuing the Ph.D. degree with the Key Laboratory of Road and Traffic Engineering of the Ministry of Education, Tongji University, Shanghai, China. His research interests include traffic signal control, connected and autonomous vehicles, and traffic congestion management.

Haoran Wang (Member, IEEE) received the bachelor's degree in transportation engineering from Tongji University, Shanghai, China, in 2017, and the Ph.D. degree from Tongji University in 2022. He is currently a Postdoctoral Researcher with the College of Transportation Engineering, Tongji University. He is a researcher on vehicle engineering, majoring in intelligent vehicle control and cooperative automation.

Dr. Wang served the IEEE TRANSACTIONS ON INTELLIGENT VEHICLES, IEEE TRANSACTIONS ON INTELLIGENT TRANSPORTATION SYSTEMS, *Journal of Intelligent Transportation Systems*, and IET *Intelligent Transport Systems* as peer reviewers with a good reputation.

Heye Huang received the B.E. degree from Central South University, Changsha, in 2018, and the Ph.D. degree from Tsinghua University in 2023. She was invited as a Visiting Scholar at the Department of Cognitive Robotics, Delft University of Technology, from 2021 to 2022. She is currently a Research Associate Fellow with Connected & Autonomous Transportation Systems Lab, University of Wisconsin–Madison. Her current research interests include connected and automated vehicles, risk assessment, decision making and motion prediction.

Dr. Huang was a recipient of Outstanding Ph.D. Graduate, Outstanding Academic Star, the National Scholarship, and the First-Class Scholarship at Tsinghua University. She received the Best Paper Award at the International Symposium on Accident Analysis & Prevention in 2021, the Journal Cover Paper Award for Engineering in 2021, the Best Research Award for Risk and Uncertainty in Engineering Systems in 2022, and the Best Paper Award at IEEE DSInS in 2023.

Xiaoguang Yang received the B.Eng. and M.S. degrees from Tongji University, Shanghai, China, in 1982 and 1988, respectively, and the Ph.D. degree in intelligent transportation systems under a joint supervision scheme in Kyoto University, Japan, in 1996. He is currently a Tenured Professor with the Key Laboratory of Road and Traffic Engineering of the Ministry of Education, Tongji University. His current research interests include transportation engineering, intelligent transportation systems, smart city and intelligent society.

Chaopeng Tan received his B.S. and Ph.D. degrees in traffic engineering from Tongji University, Shanghai, China in 2017 and 2022, respectively. He was also a visiting Ph.D. student at the University of Washington (Seattle) from 2019 to 2021 and a Postdoctoral Research Fellow with the Department of Civil and Environment Engineering, National University of Singapore from 2022 to 2024. He is currently a Postdoctoral Research Fellow with the Department of Transport and Planning, Delft University of Technology, The Netherlands. His main research interests include intelligent transportation systems, traffic modeling and control with connected vehicles, and privacy-preserving traffic control.

Jia Hu (Senior Member, IEEE) is currently working as a Zhongte Distinguished Chair of Cooperative Automation with the College of Transportation Engineering, Tongji University. Before joining Tongji University, he was a Research Associate with the Federal Highway Administration (FHWA), USA. He is an Editorial Board Member of the *Journal of Intelligent Transportation Systems* and the *International Journal of Transportation Science and Technology*. He is a member of TRB (a Division of the National Academies) Vehicle Highway Automation Committee, the Freeway Operations Committee, Simulation subcommittee of Traffic Signal Systems Committee, and the Advanced Technologies Committee of the ASCE Transportation and Development Institute. He is the Chair of the Vehicle Automation and Connectivity Committee of the World Transport Convention. He is an Associate Editor of the American Society of Civil Engineers *Journal of Transportation Engineering* and IEEE OPEN JOURNAL OF INTELLIGENT TRANSPORTATION SYSTEMS.